Check for updates

View Article Online
View Journal

CrystEngComm

Accepted Manuscript

This article can be cited before page numbers have been issued, to do this please use: D. M. Gil, M. N. Ahmed, M. Arif, H. Andleeb, S. Ali Shah, P. A. Channar, M. N. Tahir and M. Rocha, *CrystEngComm*, 2020, DOI: 10.1039/D0CE01402H.

This is an Accepted Manuscript, which has been through the Royal Society of Chemistry peer review process and has been accepted for publication.

Accepted Manuscripts are published online shortly after acceptance, before technical editing, formatting and proof reading. Using this free service, authors can make their results available to the community, in citable form, before we publish the edited article. We will replace this Accepted Manuscript with the edited and formatted Advance Article as soon as it is available.

You can find more information about Accepted Manuscripts in the Information for Authors.

Please note that technical editing may introduce minor changes to the text and/or graphics, which may alter content. The journal's standard Terms & Conditions and the Ethical guidelines still apply. In no event shall the Royal Society of Chemistry be held responsible for any errors or omissions in this Accepted Manuscript or any consequences arising from the use of any information it contains.

ROYAL SOCIETY OF CHEMISTRY

rsc.li/crystengcomm

View Article Online
DOI: 10.1039/D0CE01402H

Interplay of weak noncovalent interactions in alkoxybenzylidene derivatives of benzohydrazide and acetohydrazide: A combined experimental and theoretical investigation and lipoxygenase inhibition (LOX) studies.

Muhammad Naeem Ahmed[1*], Muneeba Arif[1], Hina Andleeb[2,3], Syed Wadood Ali Shah[4], Ifzan Arshad[2], Muhammad Nawaz Tahir[5], Mariana Rocha[6], Diego M. Gil[6,+,*]

[1]*Department of Chemistry, The University of Azad Jammu & Kashmir, Muzaffarabad 13100, Pakistan.*

[2]*Department of Chemistry, Quaid-i-Azam University, Islamabad 45320, Pakistan.*

[3]*Sulaiman Bin Abdullah Aba Al-Khail – Centre for Interdisciplinary Research in Basic Science (SA-CIRBS), Faculty of Basic and Applied Sciences, International Islamic University, Islamabad, Pakistan*

[4]*Department of Pharmacy, University of Malakand, Chakdara KPK, Pakistan*

[5]*Department of Physics, University of Sargodha, Sargodha Pakistan*

[6]*INBIOFAL (CONICET - UNT), Instituto de Química Orgánica - Cátedra de Química Orgánica I, Facultad de Bioquímica, Química y Farmacia, Universidad Nacional de Tucumán, Ayacucho 471 (T4000INI), San Miguel de Tucumán - Tucumán - Argentina*

[+] Member of the Research Career of CONICET.

*Corresponding authors:

drnaeem@ajku.edu.pk (Dr. Mudammad Naeem Ahmed).

diego.gil@fbqf.unt.edu.ar (Dr. Diego M. Gil).

Published on 07 December 2020. Downloaded by Goteborgs Universitet on 12/16/2020 11:14:45 AM.

CrystEngComm Accepted Manuscript

View Article Online
DOI: 10.1039/D0CE01402H

Published on 07 December 2020. Downloaded by Goteborgs Universitet on 12/16/2020 11:14:45 AM.

Abstract

In this study, three new hydrazide-based Schiff bases (**1-3**) have been synthesized *via* sonication in good to excellent yield 73-90% and mainly characterized by UV-visible, IR, ^{1}H-NMR and single crystal X-ray diffraction analysis. The crystal structure of compounds 1 and 2 is stabilized by N-H···O, C-H···O and C-H···N hydrogen bonds, as well as C-H···π contacts. In addition, weak π···π stacking interactions were observed in the structure of **2**. A detailed analysis of the intermolecular interactions that stabilize the crystal packing has been performed by using Hirshfeld surface analysis and energy framework calculations were carried out to analyze and visualize the topology of the supramolecular assembly, indicating that the dispersion energy is dominant over electrostatic one in the most energetic dimers of both compounds. The interaction energies associated with the noncovalent interactions observed in the crystal structures and the interplay between them have been calculated using DFT calculations. Moreover, these intermolecular interactions were also characterized by using both Bader's quantum theory of atoms in molecules (QTAIM) and NCI plots. The synthesized alkoxybenzylidene analogs of benzohydrazide and acetohydrazide were screened *in vitro* against soybean lipoxygenase and were found to show better activity than the standard indomethacin. Putative binding modes and comparison of binding interactions in the protein-ligand complex were analyzed by molecular docking studies.

Keywords: Azomethine derivatives; noncovalent interactions; Hirshfeld surfaces; DFT calculations; Energy frameworks; LOX.

1. Introduction

Schiff bases are usually synthesized from the condensation reaction of carbonyl compounds with amine derivatives. The chemical and biological significance of Schiff bases can be attributed to the presence of lone pair electrons in the sp^2 hybridized orbital of the nitrogen atom from the azomethine or imine group (-HC=N-). In addition, the metal complexes of these compounds show diverse pharmacological and biological activities including antibacterial **[1]**, antifungal **[2]** and anticancer activity **[3]**.

The chemistry of carbon-nitrogen double bond of hydrazone derivatives is fastly becoming the backbone of condensation reaction in benzo-fused *N*-heterocycles day by day **[4]**. Hydrazones constitute an important class of compounds for new drug development **[5]** and their chemical versatility is mainly attributed to the functional

CrystEngComm Accepted Manuscript

View Article Online
DOI: 10.1039/D0CE01402H

Published on 07 December 2020. Downloaded by Goteborgs Universitet on 12/16/2020 11:14:45 AM.

diversity of the azomethine –NHN=CH functional group which has nitrogen atoms with nucleophilic character, an imine carbon atom with both electrophilic and nucleophilic character and configurationally isomerism around the C=N bond. Many researchers have been synthesized these compounds as target structures and evaluated their various biological activities as well as structural properties. Hydrazides/hydrazones act as anti-micobacterial **[6]**, anti-viral, analgesic and anti-inflammatory agents **[7]**, anti-platelet, vasodilator, anti-convulsant, anti-oxidant, diuretic and anti-malarial agents. Furthermore, these compounds show anti-trypanosomal, hormone antagonist, anti-arthritis **[8]** and acetylcholinesterase inhibitor activity **[8, 9]**. In addition, many investigations have reported that Schiff bases and hydrazones show a wide range of activities including anti-inflammatory potentials **[10]**.

Noncovalent interactions have become attractive for structural chemists due to their crucial role in supramolecular chemistry, molecular recognition and materials chemistry **[11]**. The hydrogen bonding (HB) interactions are extremely important in biological systems as can be shown in nucleic acids where the assembly is controlled by a combination of H-bonds and π···π stacking interactions **[12]**. Actually, it is well-known that relatively weak intermolecular interactions such as C-H···X(X= halogens, O, S, N) hydrogen bonds play a crucial role in the crystal packing of different kinds of molecules **[13-17]**.

In light of this background, we have reported herein the synthesis and characterization of three new hydrazide based Schiff bases derivatives **1-3** (*scheme 1*). The crystal structures of compounds **1** and **2** were solved by single crystal X-ray diffractions and the computed molecular structure has been investigated by DFT calculations at B3LYP/6-311G(d,p) level of theory. We have performed a complete analysis of the intermolecular interactions which are responsible of the crystal packing by using Hirshfeld surface analysis, energy frameworks and DFT calculations. In addition, the synthesized compounds were screened *in vitro* against soybean lipoxygenase and putative binding modes and comparison of binding interactions in the protein-ligand complex were analyzed by molecular docking studies.

2. Experimental

2.1. Instrumentation. Melting points were determined on a Yanaco melting point apparatus and are reported as uncorrected. FT-IR spectra were recorded on SHIMADZU FTIR-8400S spectrophotometer using KBr disc method. Similarly, UV spectra were

CrystEngComm Accepted Manuscript

View Article Online
DOI: 10.1039/D0CE01402H

recorded on SHIMADZU UV-1601 UV-visible spectrophotometer. ^{1}H-NMR (300 MHz) spectra were measured on Bruker Avance instrument in *d*$_6$-DMSO and TMS as internal standard. Reaction progress was monitored by thin layer chromatography (TLC). 2-Hydroxybenzaldehye, 4-hydroxybenzaldehy, 1-bromopropane, 1-bromobutane and 1-bromononane were supplied by Sigma-Aldrich, whereas different carboxylic acid hydrazides were prepared according to the literature methods **[18, 19]**.

2.2. General procedure for the synthesis of 1-3. An Erlenmeyer flask was charged with 1 mmol of respective hydrazide, 1 mmol of alkoxy benzaldehyde and absolute ethanol (15 mL). 5-10 Drops of glacial acetic acid were added to catalyze the reaction. The reaction mixture was sonicated **[20]** for 2 hours at 55 ºC and progress of reaction was monitored through TLC. On completion, the reaction mixture was diluted with water and the precipitates formed were collected through filtration. The final products were purified through re-crystallization from ethanol (*scheme 1*).

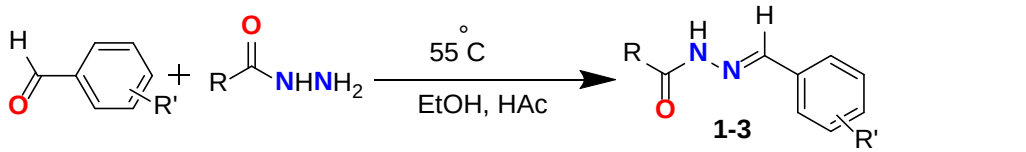

1): R = 4-MeOPh, R' = 2-Propxy

2): R = Benzyl, R' = 4-Nonoxy

3): R = 4-NO_2Ph, R' = 4-Butoxy

Scheme 1: Ultrasound assisted synthesis of compounds **1-3**.

Good quality single crystals of compounds **1-2** suitable for XRD analysis were grown from a mixture of EtOH and EtOAc (dissolving 150 mg of each compound in 5-10 mL of solvent) by slow evaporation over a period of 48 hours at ambient temperature.

***(E)-N'*-(2-Propoxybenzylidene)-4-methoxybenzohydrazide (1)**

Light brown crystals (81%); Molecular formula: $C_{18}H_{20}N_2O_3$; Molecular weight = 312.14 g/mol; m.p. = 178-180 ºC; R_F = 0.42 (*n*-Hexane: EtOAc 7:3); Solubility: $CHCl_3$/DMSO; λ_{max} = 328.14 nm; FTIR (KBrcm^{-1}): 3242 (N-H str.), 3037 (sp^2 C-H str.), 2962 and 2864 (sp^3 C-H str.), 1658 (C=O str.), 1600-1461 (C=C aromatic str.), 1508(C=N str.), 1249 and 1108 (C-O str.), 1172 (C-N str.), ^{1}H-NMR (300 MHz, DMSO-*d*$_6$): δ 8.2(s, CH), 8.1(s, NH), 7.86-6.80 (m, ArH), 3.94 (t, 2H), 3.70 (s, OCH_3), 1.73 (sext, 2H), 0.94 (t, 3H).

Published on 07 December 2020. Downloaded by Goteborgs Universitet on 12/16/2020 11:14:45 AM.

CrystEngComm Accepted Manuscript

View Article Online
DOI: 10.1039/D0CE01402H

***(Z)-N'*-(4-(Nonyloxy)benzylidene)-2-phenylacetohydrazide (2)**

Off white crystals (90%); Molecular formula: $C_{24}H_{32}N_2O_2$; Molecular weight = 380.24 g/mol; m.p. = 106-108 ºC, R_F = 0.5 (*n*-Hexane: EtOAc 7:3); Solubility:$CHCl_3$/DMSO; λ_{max} = 306.49 nm; FTIR (KBr cm^{-1}):3164 (N-H str.), 3066 (sp^2 C-H str.), 2958 and 2920 (sp^3 C-H str.), 1666 (C=O str.), 1452-1593 (C=C aromatic str.), 1544 (C=N str.), 1247 and 1014 (C-O str.), 1170 (C-N str.); ^{1}H-NMR (300 MHz, DMSO-d_6): δ 8.2 (s, 1CH), 8.0 (s, NH), 7.6-6.8 (m, 9ArH), 3.92 (t, 2H), 3.40(s, 2H), 1.70 (quin, 2H), 1.28 (m,10H), 1.30 (quin, 2H), 0.96 (t, 3H).

***(E)-N'*-(4-Butoxybenzylidene)-4-nitrobenzohydrazide (3)**

Yellow crystals (73%); Molecular formula: $C_{18}H_{21}N_3O_4$; Molecular weight = 343.15 g/mol; m.p. = 180-182 ºC, R_F = 0.43 (*n*-Hexane: EtOAc 7:3); Solubility:$CHCl_3$/DMSO; λ_{max} = 330 nm FTIR (KBr cm^{-1}): 3253 (N-H str.), 3185 (sp^2 C-H str.), 2962 and 2925 (sp^3 C-H str.), 1658 (C=O str.), 1467-1600 (C=C aromatic str.), 1521 (C=N str.), 1259 and 1064 (C-O str.), 1164 (C-N str.), ^{1}H-NMR (300 MHz, DMSO-d_6): δ 8.38-6.8 (m, 8ArH), 8.2 (s, 1CH), 8.0 (s, 1NH), 3.92 (t, 2H), 1.70 (quin, 2H), 1.30 (sext, 2H), 0.92 (t, 3H).

2.3. X-ray data collection and structure refinement. Suitable single crystals of compounds **1-2** were selected for X-ray analyses and diffraction data were collected on a Bruker Kappa APEX-II CCD detector with M_oK_α radiation at 100 K. Using the SADABS program semi emperical correction was applied **[21]**. SHELX program was also used to solve all structures by direct method **[22]**. Positions and anisotropic parameters of all non-H atoms were refined on F^2 using the full matrix least-squares technique. The H-atoms were added at geometrically calculated positions and refined using the riding model **[23]**. For compound **2**, the terminal six C-atoms of nonyl group (C16-C24) are disordered over three set of sites with occupancy ratio 0.46(2): 0.376(17): 0.17(2). All the disordered atoms are refined anisotropically with bond distance and bond angles are restrained. The atoms in each part are refined to have similar thermal parameters. Anisotropic displacement parameters of each part of individual atom are made equal to each other. The details of crystallographic data and crystal refinement parameters for the compounds **1-2** are given in **Table 1**.

2.4. Hirshfeld surface calculations. Hirshfeld surfaces and their associated two-dimensional fingerprint plots **[24-27]** were calculated by using the *CrystalExplorer17.5*

Published on 07 December 2020. Downloaded by Goteborgs Universitet on 12/16/2020 11:14:45 AM.

CrystEngComm Accepted Manuscript

View Article Online
DOI: 10.1039/D0CE01402H

program **[28]**. The normalized contact distance (d_{norm}) surface and the breakdown of two-dimensional fingerprint plots were used for identification and quantifying intermolecular interactions that are relevant in the crystal lattice. The d_{norm} function is based on both d_e (the distance from the point to the nearest nucleus external to the surface) and d_i (the distance to the nearest nucleus internal to the surface) and the van der Waals (vdW) radii of the atoms. Graphical plots of the molecular Hirshfeld surfaces mapped over d_{norm} function show a red-white-blue color scheme, where red highlights shorter contacts, white is used for contacts around the vdW separation, and blue is for longer contacts. 3D d_{norm} surfaces were mapped over a fixed color scale of -0.075 au (red)-0.75 au (blue). The shape index were mapped in the color range -1.00 au (concave) to 1.00 (convex), and curvedness in the range of -4.00 au (flat)-0.01 au (singular). The 2D fingerprint plots were generated by using the translated 0.6-2.6 Å range, and including reciprocal contacts.

Table 1: Crystallographic data and details of refinements for compounds **(1-2).**

	1	**2**
CCDC	1963584	1963585
Chemical formula	$C_{18}H_{20}N_2O_3$	$C_{24}H_{32}N_2O_2$
M_r	312.36	380.51
Crystal system, space group	Monoclinic, $P2_1/c$	Orthorhombic, $Pca2_1$
Temperature (K)	296	296
a, *b*, *c* (Å)	23.896 (8), 4.9911 (17), 13.723 (4)	9.695 (13), 24.70 (3), 9.476 (10)
β (°)	102.782 (12)	-----
V (Å^3)	1596.1 (9)	2269 (5)
Z	4	4
Radiation type	Mo *K*α	Mo *K*α
μ (mm^{-1})	0.09	0.07
Crystal size (mm)	0.38 × 0.26 × 0.16	0.38 × 0.24 × 0.20
Diffractometer	Bruker Kappa APEXII CCD	Bruker Kappa APEXII CCD
Absorption correction	Multi-scan (*SADABS*; Bruker, 2005)	Multi-scan (*SADABS*; Bruker, 2005)
T_{min}, T_{max}	0.895, 0.955	0.885, 0.965
No. of measured, independent and observed [$I > 2\sigma(I)$] reflections	18062, 3836, 2243	10378, 2195, 1090
R_{int}	0.069	0.084
$(\sin\theta/\lambda)_{max}$ (Å^{-1})	0.661	0.600
$R[F^2 > 2\sigma(F^2)]$, $wR(F^2)$, *S*	0.058, 0.138, 1.01	0.055, 0.130, 1.01
No. of reflections	3836	2195

Published on 07 December 2020. Downloaded by Goteborgs Universitet on 12/16/2020 11:14:45 AM.

CrystEngComm Accepted Manuscript

View Article Online
DOI: 10.1039/D0CE01402H

No. of parameters	210	291
No. of restraints	121	130
H-atom treatment	H-atom parameters constrained	H-atom parameters constrained
$\Delta\rangle_{max}$, $\Delta\rangle_{min}$ (e Å^{-3})	0.18, -0.20	0.13, -0.14

2.5. Interaction energies and energy framework analysis. To calculate, visualize and analyse the 3D energy frameworks along with the intermolecular interaction energies we have used the CrystalExplorer17.5 software. The single point molecular wavefunction at B3LYP/6-31G(d,p) level of theory is used to calculate the energy by generating a cluster of radius 3.8 Å around the molecule. The neighbouring molecules in the shell around the central molecule are generated by applying crystallographic symmetry operations **[29, 30].**

2.6. Computational details. The overall quantum chemical calculations for compounds **1-2** were performed by using the Gaussian09 software **[31]**. The molecular structure of the compounds were optimized using single crystal XRD geometries at B3LYP/6-311G(d,p) level of theory **[32, 33]**. The frequency analysis was also carried out with the same level of theory for verification of stability related with optimized geometries. Electronic transitions were computed within the Time-Dependent Density Functional Theory (TD-DFT) **[34]** taking into account implicitly the solvent effect (ethanol).

To compute the interaction energies in the solid state we have used the crystallographic coordinates at the B3LYP-D3/def2-TZVP level of theory. The D3 Grimme's dispersion correction was used for an adequate evaluation of non-covalent interactions where dispersion effects are relevant **[35]**. The quantum theory of atoms in molecules (QTAIM) analysis **[36]** has been carried out at the same level of theory and using the AIM2000 program **[37]**. The NCI plot isosurfaces were also used to characterize the non-covalent interactions **[38]**. These surfaces indicate favorable and unfavorable interactions, as differentiated by the sign of the second density Hessian eigenvalue and defined by the isosurface color. The color scheme is red-yellow-green-blue with red for repulsive and blue for attractive.

2.7. In vitro Lipoxygnase inhibition studies (1-3). Soybean lipoxygenase enzyme has been used as an in-vitro biochemical model for the determination of anti-inflammatory potentials **[39]**. Similarly, indomethacin was used as reference drug. The lipoxygenase

Published on 07 December 2020. Downloaded by Goteborgs Universitet on 12/16/2020 11:14:45 AM.

CrystEngComm Accepted Manuscript

View Article Online
DOI: 10.1039/D0CE01402H

activity of synthesized compounds (**1-3**) was determined by spectrophotometric method with slight modification **[40]**. Inhibition was determined by measuring the loss of soybean 15-LOX activity (5 μg) with 0.2 μM linoleic acid as the substrate prepared in borate buffer (0.2 M, pH 9.0). The inhibition in triplicate at various concentrations of synthetic compounds were recorded at 234 nm using UV-Vis spectrophotometer. Indomethacin was used as positive control, while methanol was used as negative control **[41]**. IC_{50} indicating the concentration of 50% inhibition was calculated. Soybean lipoxygenase inhibition data is reported in IC_{50} values.

2.8. Molecular modeling study. All docking studies were performed using Autodock Vina (ver. 1.5.6) **[42].** For this purpose, the crystal structure of soybean lipoxygenase complexed with 13-(S)-hydroproxy-9(Z)-2,11(E)-octadecadienoic acid (code ID: 1IK3) were retrieved from protein data bank. The co-crystallized ligand and water molecules were removed, and the protein was converted to pdbqt format using Autodock Tools **[43].** The 2D structures of ligands were sketched using Chemdraw 12.0. the 2D structures were converted to 3D format by Openbabel (ver. 2.3.1) **[44]**. PDBQT files were prepared in MGL Tools **[43].** The docking parameters were set as follows: size_x = 40; size_y = 40; size_z = 40; center_x = 27.458; center_y = 4.218; center_z = 15.623. The other parameters were left as default. Finally, the conformations with the most favorable free energy of binding were selected for analyzing the interactions between the target enzyme and inhibitors. PyMOL version 1.8.8.2 **[45]** and Chimera 1.6 software **[46]** was used for 3D molecular graphics, structural alignments and visualizations. Physicochemical properties were calculated using SwissADME **[47].**

3. Results and discussion

3.1. *Synthesis and characterization*

The compounds under study were synthesized by a procedure simple and faster. Equimolar quantities of the respective hydrazine and alkoxy benzaldehyde in ethanol as solvent in the presence of acetic acid, react by sonication during 2 hours at 55 ºC leading the corresponding hydrazone derivatives (**1-3**). Re-crystallization from ethanol affords the products **1** and **2** as crystalline solids in good yields. For **3**, only very small and twinned crystals with low X-ray scattering ability were obtained.

The IR spectra of compounds **1-3** are shown in **Figure S1, ESI**. The main features associated with the hydrazone moiety, -C(O)-NH-N=C- will be discussed. The medium

Published on 07 December 2020. Downloaded by Goteborgs Universitet on 12/16/2020 11:14:45 AM.

CrystEngComm Accepted Manuscript

View Article Online
DOI: 10.1039/D0CE01402H

intensity band at 3233, 3235 and 3233 cm^{-1} for **1**, **2** and **3**, respectively are assigned to *ν*(N-H) stretching mode. The *ν*(C=O) stretching mode is observed at 1656 cm^{-1} in the IR spectrum of **1** (calculated 1710 cm^{-1}) and as a strong infrared absorption at 1666 cm^{-1} for compound **2** (calculated 1730 cm^{-1}). The *ν*(C=O) stretching vibration is located at 1658 cm^{-1} in the IR spectra of **3**. The *δ*(N-H) bending mode of the amide group, in general appears as a very intense absorption in the 1600-1500 cm^{-1}. The IR spectra show medium intensity absorptions at around 1535, 1559 and 1561 cm^{-1} for **1**, **2** and **3**, respectively, in agreement with related compounds **[48]**. The weak bands located at 1124 for **1**, 1147 cm^{-1} for **2** and 1139 cm^{-1} for **3** are assigned to the *ν*(N-N) stretching mode. Finally, the band corresponding to the *ν*(C=N) stretching mode in Schiff bases is generally observed in the range 1650-1600 cm^{-1} **[3, 17]**. For the studied compounds, we have assigned this mode to the absorptions observed at 1648, 1643 and 1651 cm^{-1} for **1**, **2** and **3**, respectively.

The electronic spectra of compounds **1-3** are shown in **Figure S2, ESI**. The absorption bands at 327 and 307 and 332 nm for **1**, **2** and **3**, respectively are assigned to HOMO-LUMO electronic transitions with $\pi \rightarrow \pi^*$ nature.

The ^{1}H NMR (300 MHz, d_6-DMSO) data for compounds **1-3** show singlet signals in the δ = 8.0-8.1 ppm range, corresponding to the N-H protons of the amide group. The singlet at δ = 8.2 ppm observed in the spectra of all compounds is assigned to the proton of the azomethine moiety. The protons of the aromatic rings are observed in the region δ = 8.38-6.80 ppm.

3.2. *Description of crystal structures of compounds 1-2.*

Although the main difference between the compounds are simply the substituents and their substitution positions, the resulting conformations, crystal systems and space groups of both compounds are different. The crystallographic study showed that compound **1** crystallizes in the monoclinic form with $P2_1/c$ space group, whereas **2** exists in the orthorhombic crystal system, space group $Pca2_1$. Both compounds accommodate four molecules per unit cell.

Figure 1a and **2a** show a view of the molecular structure of compounds **1** and **2**, respectively. Selected X-ray bond lengths and angles, together with the computed values at B3LYP/6-311G(d,p) approximation are shown in **Table 2**. The optimized molecular structure of both compounds are shown in **Figures S3-S4, ESI**. In the crystal structure of **1**, the 4-methoxybenzene moiety A (C1-C7/O1), the linker moiety 1-methyl-2-methylenehydrazine B (C8/N1/N2/C9), phenyl ring C (C10-C15) and propanoxy group

Published on 07 December 2020. Downloaded by Goteborgs Universitet on 12/16/2020 11:14:45 AM.

CrystEngComm Accepted Manuscript

View Article Online
DOI: 10.1039/D0CE01402H

D (O3/C16-C18) are planar with r. m. s. deviation of 0.0103, 0.0063, 0.0101 and 0.0788 Å, respectively. The carbonyl O-atom is at a distance of 1.525(6) Å and -1.035 (5) Å from the mean planes A and B, respectively. The dihedral angles between A/B, B/C and C/D are 30.99(18)°, 29.41(18)° and 12.74(14)°, respectively. The moiety A and C are twisted at 14.32(12)°, associated with different packing interactions. In **2** (Figure 2a), the terminal C-atoms of the nonoxy group are disordered. The disorder is resolved for last four C-atoms with occupancy ratio of 0.54(2): 0.46(2). The benzyl group A (C1-C7), the linker moiety B (C8/N1/N2/O1) and the part of 4-methyl phenol part C (C9-C15/O2) are planar with r.m.s. deviation of 0.0165, 0.0022 and 0.0105 Å, respectively. The dihedral angle between A/B, A/C and B/C is 69.72(18)°, 86.93(13)° and 28.92(27)°, respectively.

As shown in Table 2, the imine N2-C9 bond lengths are 1.272(3) and 1.271(6) Å for **1** and **2**, respectively. These bond lengths are significantly shorter than N1-N2 and N1-C8 bond lengths in agreement with the typical N2=C9 double bond character. The C9-C10 bond lengths are 1.470(3) Å for **1** and 1.452(7) Å for **2**, which are indicative of the single bond character of this bond. The bond angle N1-N2-C9 are 115.2(2)º for **1** and 114.9(4)º for **2**, which are significantly smaller than the ideal value of 120º expected for N-atoms sp^2-hybridized. This is probably a consequence of repulsion between the nitrogen lone pairs and the adjacent N-N bond. The C=O bond lengths are similar for both compounds, with values of 1.223(3) and 1.220(6) Å for **1** and **2**, respectively. These results indicate that the C=O bond length is not influenced with the substituents. The C-O bond length corresponding to 2-propoxy in **1** is slightly longer (1.368 Å) in comparison with the C-O distance in the 4-nonoxy substituent in 2 (1.362 Å), demonstrating a smaller π-donating effect of the alkoxy O-atom against the aromatic ring.

In accordance with Table 2, a good agreement between experimental and computed geometrical parameters has been observed. It is important to mention that the calculations were carried out in gas phase where the crystal packing effects are completely ignored. Notably, the larger discrepancies are observed for the C8-N1 and N1-N2 bonds, which errors are about 0.03 and 0.023 Å, respectively. Calculated and experimental angles and dihedral angles are in very good agreement indicating that both molecules undergo small changes due to intermolecular interactions, as shown in the calculated and experimental molecular structures.

Published on 07 December 2020. Downloaded by Goteborgs Universitet on 12/16/2020 11:14:45 AM.

CrystEngComm Accepted Manuscript

View Article Online
DOI: 10.1039/D0CE01402H

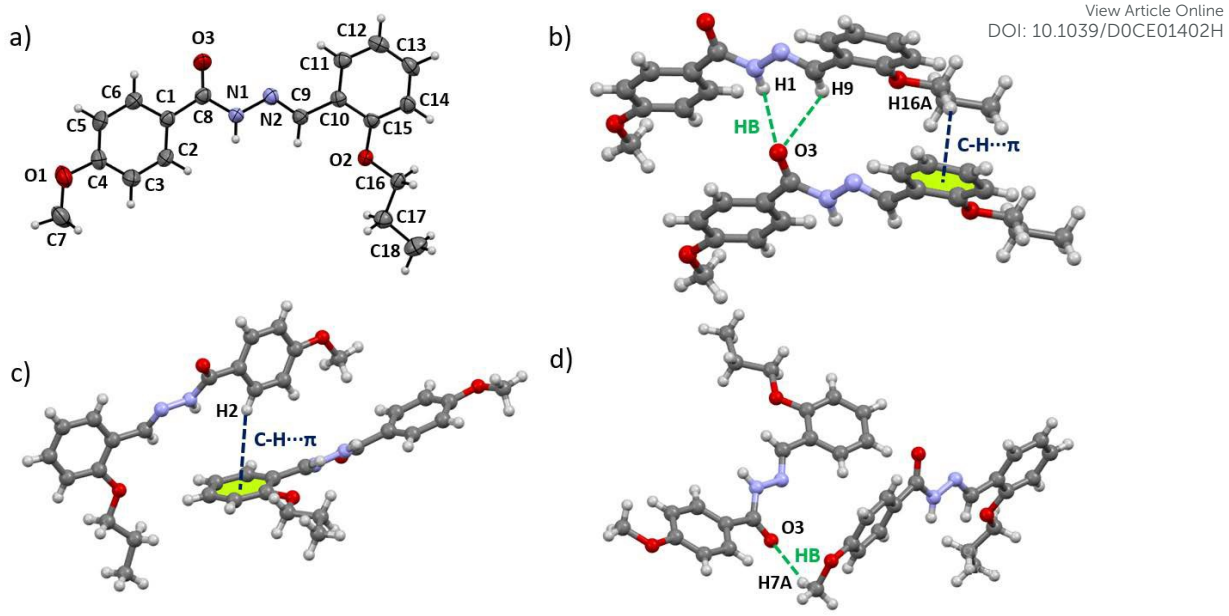

Figure 1. a) ORTEP diagram of **1** at 30 % probability level along with the numbering scheme; **b)** dimer of **1** (Motif 1, **M1**) showing the formation of N-H···O, C-H···O hydrogen bonds and C-H···π interactions; **c)** formation of intermolecular C-H···π interactions (**M2**), d) dimer of **1** stacked through C-H···O hydrogen bonds (**M3**).

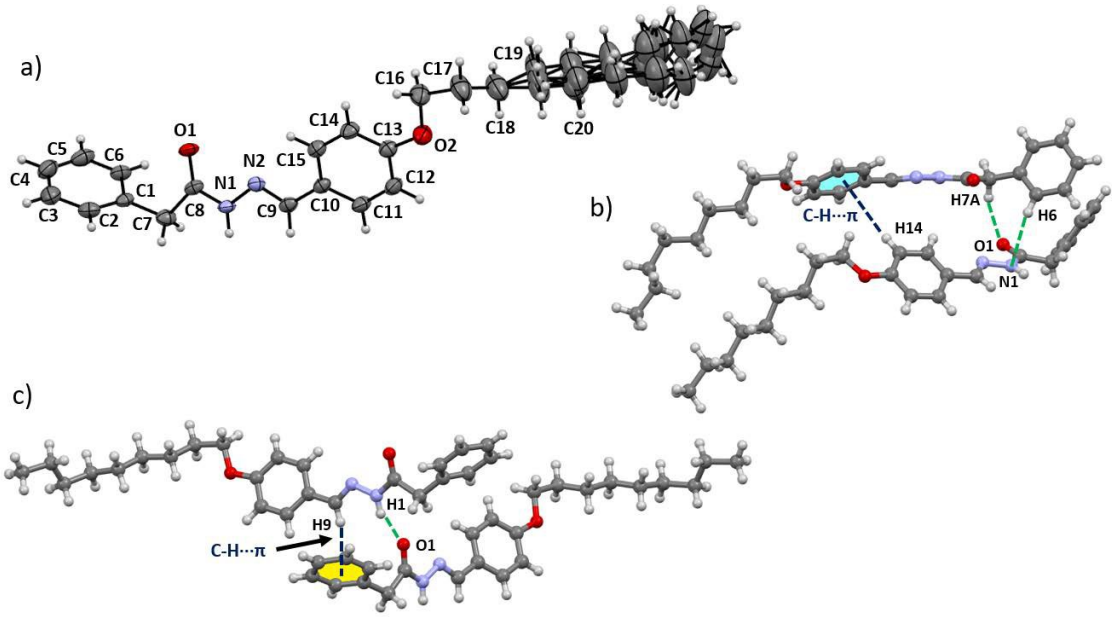

Figure 2. a) ORTEP diagram of **2** with ellipsoids at 30% probability level with non H-atoms numbering scheme. The molecular structure reveals disorder in the alkyl chain; **b)** Structural motif showing a combination of C-H···O and C-H···N hydrogen bonds (green dashed lines) and C-H···π (blue dashed lines) interactions; **c)** Formation of N-H···O hydrogen bonds and C-H···π interactions. In Fig. 2b and 2c, only the major occupancy disordered atoms are shown (see text).

Published on 07 December 2020. Downloaded by Goteborgs Universitet on 12/16/2020 11:14:45 AM.

CrystEngComm Accepted Manuscript

View Article Online
DOI: 10.1039/D0CE01402H

Table 2. Selected experimental and computed geometrical parameters (Å, º) for compounds **1-2**.

Parameters	Compound 1		Compound 2	
	Exp.	Calcd.[a]	Exp.	Calcd.
C1-C8	1.486(3)	1.498	-	-
C7-C8	-	-	1.501(7)	1.531
C8-O3	1.223(3)	1.212	-	-
C8-O1	-	-	1.220(6)	1.209
C8-N1	1.358(3)	1.390	1.356(6)	1.383
N1-N2	1.378(3)	1.355	1.381(6)	1.358
C9-N2	1.272(3)	1.281	1.271(6)	1.279
C9-C10	1.470(3)	1.463	1.452(7)	1.460
C4-O1	1.368(3)	1.359	-	-
C15-O2	1.368(3)	1.365	-	-
C13-O2	-	-	1.362(7)	1.359
C1-C8-N1	115.2(2)	114.3	-	-
C7-C8-N1	-	-	112.6(4)	113.1
C8-N1-N2	119.9(2)	121.0	121.5(4)	121.5
N1-N2-C9	115.2(2)	117.2	114.9(4)	117.4
N2-C9-C10	120.2(2)	121.1	121.4(4)	122.2
C1-C8-N1-N2	-178.5(2)	177.7	-	-
C7-C8-N1-N2	-	-	179.8(4)	177.1
C8-N1-N2-C9	178.8(2)	173.7	-170.5(4)	-176.8
N1-N2-C9-C10	-173.9(2)	179.6	179.6(4)	179.6

[a] Calculated at B3LYP/6-311G(d,p) level of theory.

The geometrical parameters of the hydrogen bonding interactions for compounds **1** and **2** are displayed in **Table 3**. The molecule of **1** has a methoxy substituent on the arene ring (C1-C6) in the *para*-position (see Fig. 1a). In the crystal packing of **1**, the molecules are connected with each other in the form of dimers through N1-H1···O3 and C9-H9···O3 interactions, where O3 atom from the carbonyl group acts as acceptor (Figure 1b). The former is the strongest interaction as reflected by the geometrical parameters reported in Table 3. The stabilization of the crystal structure is also supported by the presence of weak C-H···O interactions involving the O3 from the carbonyl as acceptor and the H7A of the methoxy group located in the *para*-position in the benzohydrazide moiety (Figure 1c). In addition, the molecule of **2** has a propoxy group located at the *orto* position of the phenyl ring (C10-C15). This propoxy group is involved in C-H···π interactions of the type C16-H16A···Cg2 [d(H16···Cg2) = 2.63 Å, <(C16-H16A···Cg2) = 151º] (Figure 1a). The structure is also stabilized by C2-H2···Cg2 [d(H2···Cg2) = 3.22 Å, <(C2-H2···Cg2)

Published on 07 December 2020. Downloaded by Goteborgs Universitet on 12/16/2020 11:14:45 AM.

CrystEngComm Accepted Manuscript

View Article Online
DOI: 10.1039/D0CE01402H

= 156º] (Figure 1b) involving the phenyl ring Cg2 (C10-C15). The phenyl rings are not involved in π···π stacking interactions, as compared with the packing of **2** (see below).

Table 3. Geometrical parameters (Å, º) of hydrogen bonds in compounds **1** and **2**.

D-H···A	D-H	H···A	D···A	<(D-H···A)
Compound 1				
N1-H1···O3^{i}	0.86	2.16	2.916(2)	146.1
C9-H9···O3^{i}	0.93	2.67	3.349(2)	130.6
C7-H7A···O3^{ii}	0.96	2.64	3.530(2)	153.8
Compound 2				
N1-H1···O1^{iii}	0.86	2.17	2.918(3)	145.9
C7-H7A···O1^{iv}	0.97	2.58	3.521(3)	162.9
C6-H6···N1^{iv}	0.93	2.72	3.546(3)	147.8

Symmetry codes: (i) x, y+1, z; (ii) x, -y-1/2, +z-1/2; (iii) x+1/2, -y, z; (iv) –x+1/2+1, y, +z-1/2.

The crystal packing of **2** exhibits an interesting structural pattern characterized by different structural motifs. The amide O1 and N1 atoms act as acceptors forming C7-H7A···O1 [d(H7···O1) = 2.583(3) Å] and C6-H6···N1 [d(H6···N1) = 2.724(2) Å] hydrogen bonds (Figure 2b). The C-H···N hydrogen bonds are absent in the crystal packing of **1** because the orientation of the benzyl moiety favors this interaction. In addition, this structural motif is also stabilized by C-H···π interactions (C14-H14···Cg2) with inter-centroid H14···Cg2 distance of 3.415 Å (Figure 2b). As shown in Figure 2c, the supramolecular assembly of **2** is governed by N1-H1···O1 hydrogen bonds [d(H1···O1) = 2.165(2) Å] and C-H···π interactions involving the H9 atom of the azomethine group and the Cg1 (C1-C6) centroid. The crystal packing of **2** shows weak π···π stacking interactions between the Cg1 (C1-C6) and Cg2 (C10-C16) centroids, with Cg1···Cg2 inter-centroid distance of 4.817(6) Å (symmetry code: 1-x,-y, -1/2+z).

3.3. *Hirshfeld surface analysis*

Hirshfeld surface analyses have been carried out in order to get further insights into the packing motifs and the contributions of the main intermolecular interactions that are responsible for the crystal stabilization of compound **1**. We have not performed Hirshfeld surface analysis of compound **2** due to the molecular disorder observed. Recently, Hirshfeld surface analysis for different hydrazide Schiff bases were evaluated for a better comprehension of their crystal packing **[49]**. **Figure 3a** shows Hirshfeld surfaces mapped over d_{norm} function in two orientations. The corresponding full two-dimensional

Published on 07 December 2020. Downloaded by Goteborgs Universitet on 12/16/2020 11:14:45 AM.

CrystEngComm Accepted Manuscript

View Article Online
DOI: 10.1039/D0CE01402H

fingerprint plots and resolved to show H···C/C···H and H···O/O···H contacts are displayed in **Figure 3b**.

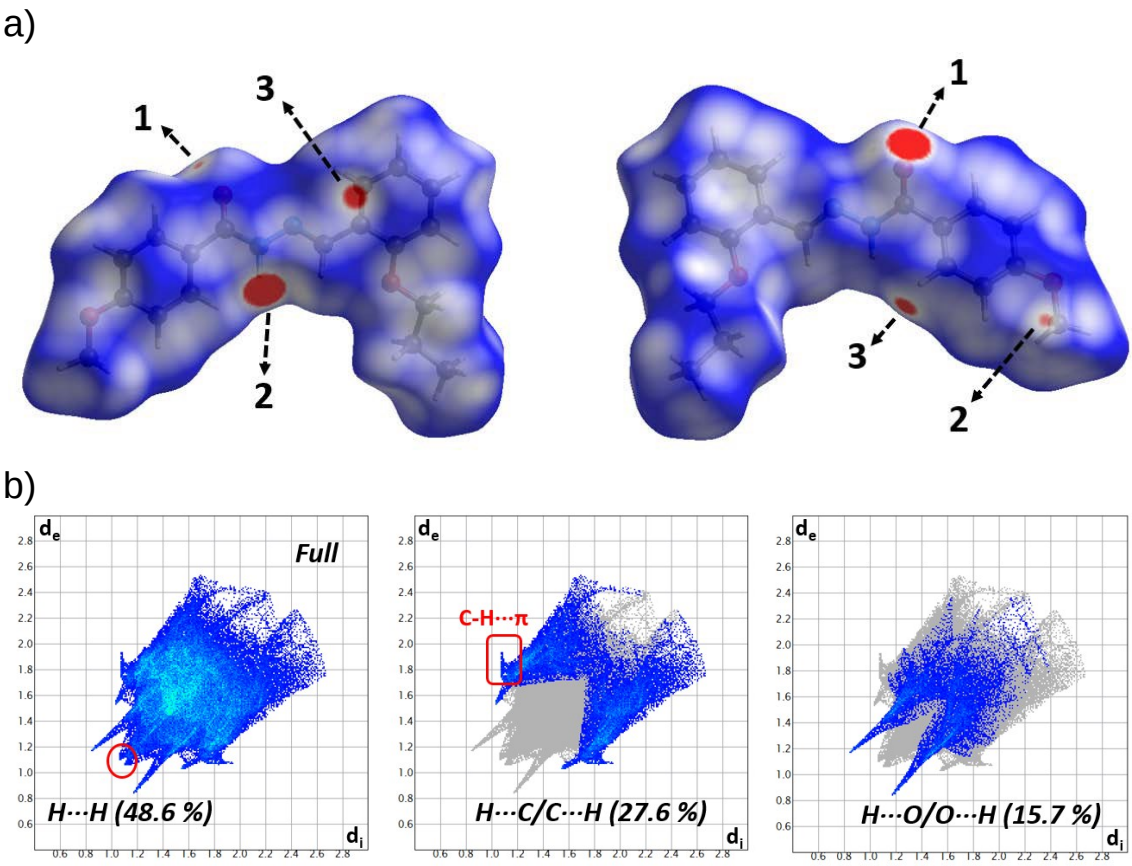

Figure 3. (a) Hirshfeld surfaces of **1** mapped over d_{norm} property in two orientations: The second molecule rotated 180º around the vertical axis of the plot. The labels are discussed in the main text. **(b)** Full and decomposed two dimensional fingerprint plots for compound **1** showing percentage contributions to the total Hirshfeld surface area of the molecules.

H···H contacts represent the largest contribution (48.6 %) to the Hirshfeld surface area, and they are highlighted in the middle of scattered points in the fingerprint plots at (d_e + d_i) ≈ 2.4 Å, which is the sum of the vdW radii.

The two larger red spots labeled 1 in the d_{norm} surfaces of **1** are attributed to N-H···O hydrogen bonds, involving the O3 atom as acceptor. Another red areas labeled 2 in the surfaces are due to the formation of C-H···O hydrogen bonds between the H7A of the methoxy substituent and the O-atom from the carbonyl group. These type of interactions have been evaluated extensively in dihydropyrimidine-2(1*H*)-thione derivatives and in 1-

Published on 07 December 2020. Downloaded by Goteborgs Universitet on 12/16/2020 11:14:45 AM.

CrystEngComm Accepted Manuscript

View Article Online
DOI: 10.1039/D0CE01402H

(adamantine-1-carbonyl)-3-substituted thioureas **[50]**. The H···O/O···H contacts are also visible in the fingerprint plots (Figure 3b) as a pair of symmetrical sharp spikes at (d_e + d_i) ≈ 2.1 Å and contribute 15.7% to the total Hirshfeld surface area.

The presence of H···C/C···H contacts are easily visible in the d_{norm} maps as red regions labeled 3 for compound **1**. The spot labeled 3 is attributed to C-H···π interactions involving the centroid Cg2 (C10-C15) and the H2 atom from a neighboring molecule (H2···Cg2 distance of 3.22 Å). These features support the importance of the C-H···π interactions in the supramolecular assembly of compound **1**. These interactions are also visible as a pair of wings in the top left and bottom right region of the 2D fingerprint plots (indicated by red encircles in Figure 3b), with the shortest (d_e + d_i) ≈ 3.0 Å. Furthermore, the shape of the wings and the sum of d_e and d_i are indicative of the relevance of the C-H···π interaction.

3.4. *Interactions energies and energy frameworks*

In order to describe the intermolecular interactions in a whole-of-molecule approach, we have analyzed the separate electrostatic and dispersion contributions to the total interaction energy. The interactions were calculated using the B3LYP/6-31G(d,p) energy model implemented in *CrystalExplorer17.5* program. In the calculation, the total energy is modelled as the sum of the electrostatic (E_{ele}), polarization (E_{pol}), dispersion (E_{dis}) and exchange-repulsion (E_{rep}) terms **[30, 51]**. The main intermolecular interactions observed in the crystal structure of compound **1** are listed in **Table 4** along with the respective interaction energies.

The highest total energy of -71.6 kJ/mol corresponds to a molecular pair (Motif 1, Figure 1b) formed by the bifurcated N1-H1···O3 and C9-H9···O3 hydrogen bonds, being the N1-H1···O3 the strongest interaction, in accordance with the geometrical parameters reported in Table 3 and 4. This motif is further supported by presence of C-H···π interactions involving the H16A of the methylene group and the Cg2 centroid. The dispersion (58.96%) and electrostatic (41.08%) energies contribute towards the stabilization of this molecular pair. Motif 2 is established through an intermolecular C2-H2···Cg2 interaction resulting in the overall stabilization energy of -41.4 kJ/mol, with 72.13% contribution from dispersion component towards stabilization. Motif 3 is stabilized by the presence of weak intermolecular C-H···O interactions involving the H7A of the methoxy group and the O3 atom (Figure 1d), [E_{tot} = -28.4 kJ/mol with contributions of 64.5% dispersion energy and 35.49% electrostatic energy].

Published on 07 December 2020. Downloaded by Goteborgs Universitet on 12/16/2020 11:14:45 AM.

CrystEngComm Accepted Manuscript

View Article Online
DOI: 10.1039/D0CE01402H

Published on 07 December 2020. Downloaded by Goteborgs Universitet on 12/16/2020 11:14:45 AM.

Table 4. Intermolecular interactions along with the geometrical parameters (Å, º) and respective interaction energies (E_{tot}) partitioned into electrostatic (E_{ele}), polarization (E_{pol}), dispersion (E_{dis}) and exchange-repulsion (E_{rep}) energy components. The energy values are expressed in kJ/mol.

Motif	Symmetry	Interactions	d(H···A/Cg), <(D-H···A)[a]	E_{ele}	E_{pol}	E_{dis}	E_{rep}	E_{tot}
Compound 1								
M1	x, y, x	N1-H1···O3	2.643, 154	-38.2	-13.1	-73.7	68.9	-71.6
		C9-H9···O3	2.668, 131					
		C16-H16A···Cg2	2.630, 151					
M2	x, -y+1/2, z+1/2	C2-H2···Cg2	3.220, 156	-15.5	-3.20	-48.4	31.8	-41.4
M3	x, -y+1/2, z+1/2	C7-H7···O3	2.643, 154	-9.20	-6.10	-27.8	16.3	-28.4

[a] Geometrical parameters of hydrogen bonds (Å, º) and H···Cg distance (Å), Cg1 and Cg2 are the centroids of the C1-C6 and C10-C16 rings, respectively.

Figure 4 shows graphically the 3D topology of interactions energies in the form of energy frameworks, which provide a view of supramolecular assembly of crystals through cylinders joining centroids of molecular pairs by using red, green and blue color codes for the components electrostatic, dispersion and total energy, respectively. The radius of the cylinders is proportional to the magnitude of the interaction energies.

For compound **1**, the partial sum of dispersion energies (-149.9 kJ/mol) is greater than that electrostatic ones (-62.9 kJ/mol), which evidences a clear dominance of dispersion energy over the electrostatic component. This observation is in agreement with the higher diameter of the cylindrical tubes for dispersion interaction in comparison to that of the electrostatic counterpart along the *a*-axis, as shown in Figure 4.

Compound 1

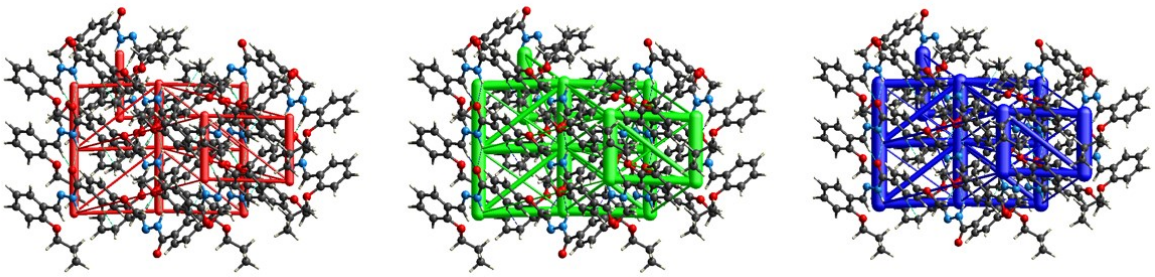

Figure 4. Energy frameworks along *a*-axis for compound **1**, showing the electrostatic (left, red), dispersion (middle, green) and total interaction energy (right, blue). The energy scale factor of 90 kJ/mol was used with a cut-off value of 5 kJ/mol.

CrystEngComm Accepted Manuscript

View Article Online
DOI: 10.1039/D0CE01402H

Published on 07 December 2020. Downloaded by Goteborgs Universitet on 12/16/2020 11:14:45 AM.

3.5. *Theoretical study*

The theoretical study performed in this work is mainly focused to the analysis of hydrogen bonds and C-H···π interactions observed in the crystal structure of compounds **1** and **2**. These interactions were studied by using NCI plots and QTAIM analysis. These interactions play a crucial role in the biological properties observed for these compounds which were correlated with docking studies (see below).

The molecular electrostatic potential (MEP) surfaces of **1** and **2** are shown in **Figure 5**. In both compounds, the most negative region is located at the O-atom from the carbonyl group, with MEP values of -194 and -189 kJ/mol for **1** and **2**, respectively. The most positive values are observed at the H-atoms from the amide group. Therefore, the hydrogen bonding interactions between both groups is strongly favored electrostatically.

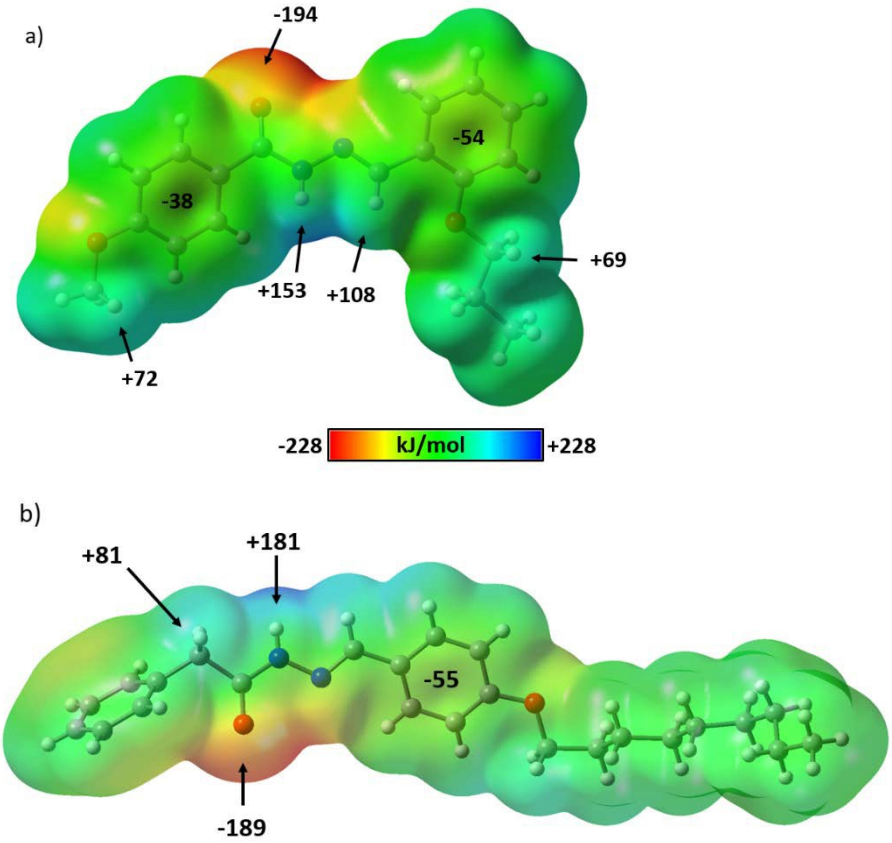

Figure 5. MEP surfaces of compounds **1** (a) and **2** (b) plotted onto the 0.001 a.u. isosurface. The values at the selected points on the surface are given in kJ/mol.

CrystEngComm Accepted Manuscript

View Article Online
DOI: 10.1039/D0CE01402H

Published on 07 December 2020. Downloaded by Goteborgs Universitet on 12/16/2020 11:14:45 AM.

Interestingly, the MEP values are also negative over the aromatic rings in both compounds, thus both π-systems could interact with positive regions such as aliphatic and aromatic H-atoms to form C-H···π interactions.

We have selected the hydrogen bonding network shown in Figures 1 and 2 to analyze the energetic features in both compounds. For simplicity, in the first theoretical model used for the analysis (Fig. 6a), we have replaced the 4-methoxyphenyl ring by a methyl group (red arrow) and we have reduced by one the number of methylene groups in the propoxy moiety of **1**. It shows a moderately strong dimerization energy (ΔE_1 = -64.2 kJ/mol) due to the formation of N-H···O and C-H···O hydrogen bonds. Interestingly, this motif is also stabilized by C-H···π interactions. In the second model of **1** (Fig. 6b), we have replaced the 2-propoxyphenyl ring by a methyl group. In this dimer, the dimerization energy is reduced to ΔE_2 = -26.2 kJ/mol due to the presence of C-H···O hydrogen bonds.

For compound **2**, the theoretical models used consist in the replacing of the -O-$(CH_2)_8$-CH_3 group by an H-atom, indicated by a red arrow in Figures 6c. In the first model of **2** (Fig. 6c), a combination of C-H···O, C-H···N and C-H···π interactions are formed, with a dimerization energy of ΔE_3 = -55.8 kJ/mol. The dimerization energy of the second model (Fig. 6d) is somewhat greater that of the first model due to the presence of a combination of a strong N-H···O hydrogen bonds with C-H···π interactions involving the H-atom of the azomethine group. These results are in agreement with the interaction energies obtained from the crystal structure (see Table 4) by using the CrystalExplorer17.5 program.

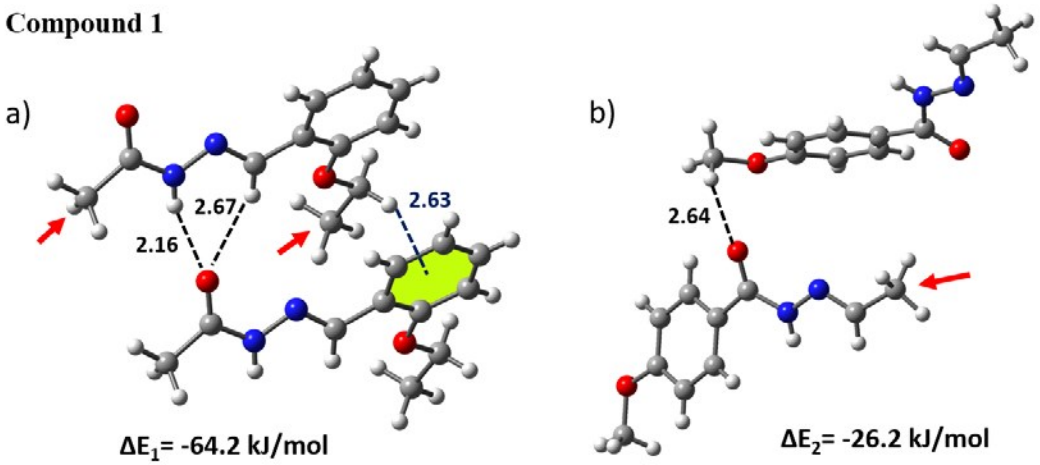

CrystEngComm Accepted Manuscript

View Article Online
DOI: 10.1039/D0CE01402H

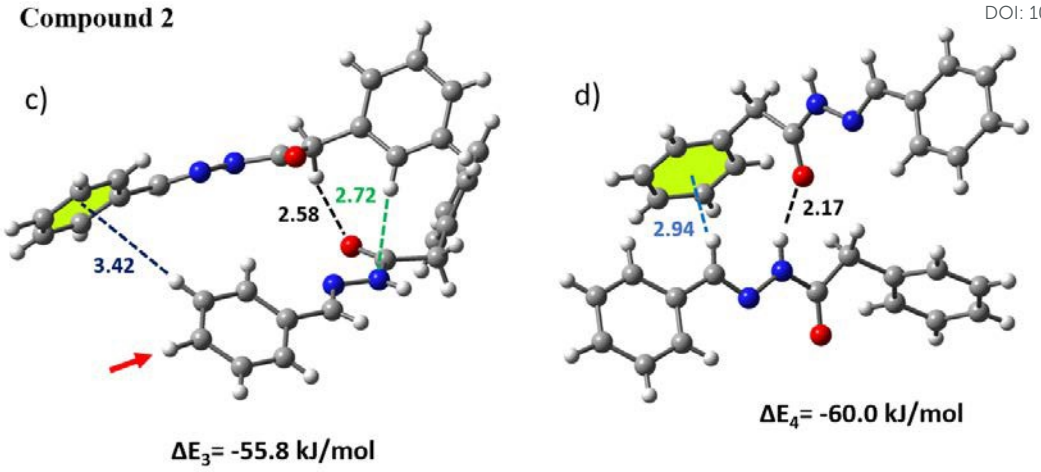

Figure 6. (a, b) Dimers of models of compound **1** showing hydrogen bonds and C-H···π interactions, distances in Å. **(c, d)** Dimers of theoretical models of compound **2**.

In order to characterize the C-H···π and hydrogen bonding interactions, we have computed the NCI plots using the B3LYP-D3/def2-TZVP wavefunction. The NCI plot is an important tool to visualize the effectiveness of the non-covalent interactions. The color scheme is a red-yellow-green-blue scale with red (repulsive) and blue (attractive) regions. Yellow and green surfaces indicate weak repulsive and weak attractive interactions, respectively. **Figure 7** shows a NCI plot for the first theoretical model of **1** showed in Fig. 6a. The presence of large green isosurface located between the methylene group and the phenyl ring confirms the existence of C-H···π interactions. The light blue isosurface located between the O-atom from the carbonyl group and the N-H moiety is an indicative of a strong hydrogen bond between both groups. To characterize these hydrogen bonding interactions, we have used the Bader's quantum theory of atoms in molecules (QTAIM) **[36]**. The distribution of bond critical points (BCP) and bond paths of the N-H···O and C-H···O hydrogen bonds is highlighted in the right panel of Figure 7. In this representation we have observed the presence of two BCP (represented by red spheres) and bond paths connecting the O-atom from the carbonyl group with the H-atoms of the N-H and C-H moieties. The values of charge density and interaction energy are also indicated in **Figure 7**. These values are within the range 0.002-0.04 a.u. proposed by Koch and Popelier **[52]** for hydrogen bonding interactions. The charge density of BCP1 (N-H···O H-bond) is the largest one indicating the stronger interaction compared with C-H···O hydrogen bond (BCP2). The interaction energy of each hydrogen bonding contact can be estimated according to the approach proposed by Emamian and co-workers **[53]**.

Published on 07 December 2020. Downloaded by Goteborgs Universitet on 12/16/2020 11:14:45 AM.

CrystEngComm Accepted Manuscript

View Article Online
DOI: 10.1039/D0CE01402H

The energies are indicated in Figure 7, and they evidence that the contribution of N-H···O is -10.10 kJ/mol and that the C-H···O bonds involving the H-atom of the imine group is significantly smaller (-2.743 kJ/mol).

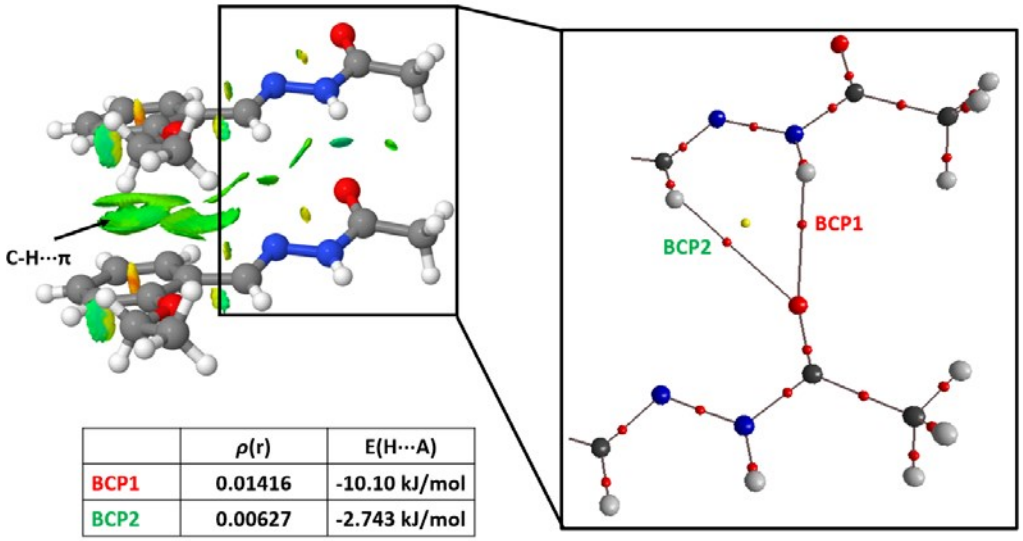

	ρ(r)	E(H···A)
BCP1	0.01416	-10.10 kJ/mol
BCP2	0.00627	-2.743 kJ/mol

Figure 7. Left: NCI surface of a dimer of compound **1**. The gradient cut-off is 0.35 a.u. and the color scale is -0.4 < ρ < +0.4 a.u. Right: QTAIM distribution of bond and ring critical points (red and yellow spheres, respectively) and bond paths calculated at B3LYP-D3/def2-TZVP level of theory of the H-bonded fragment.

The NCI plot index surfaces obtained for both theoretical dimers of compound **2** are shown in **Figure 8**. For the first dimer (Fig. 8a), the C-H···π interactions are characterized by green isosurfaces located between the π-cloud of the phenyl ring and the aromatic H-atom of other molecule. In addition, the NCI plot also reveals the existence of C-H···O and C-H···N hydrogen bonds. Similar features were observed for the second dimer of **2** (Fig. 8b), in which the C-H···π interaction is also confirmed by the green isosurface located between the H9 atom from the azomethine moiety and the phenyl ring. For the later dimer, the N-H···O hydrogen bond is characterized by small blue isosurfaces located between the O-atom and the amino groups.

Published on 07 December 2020. Downloaded by Goteborgs Universitet on 12/16/2020 11:14:45 AM.

CrystEngComm Accepted Manuscript

View Article Online
DOI: 10.1039/D0CE01402H

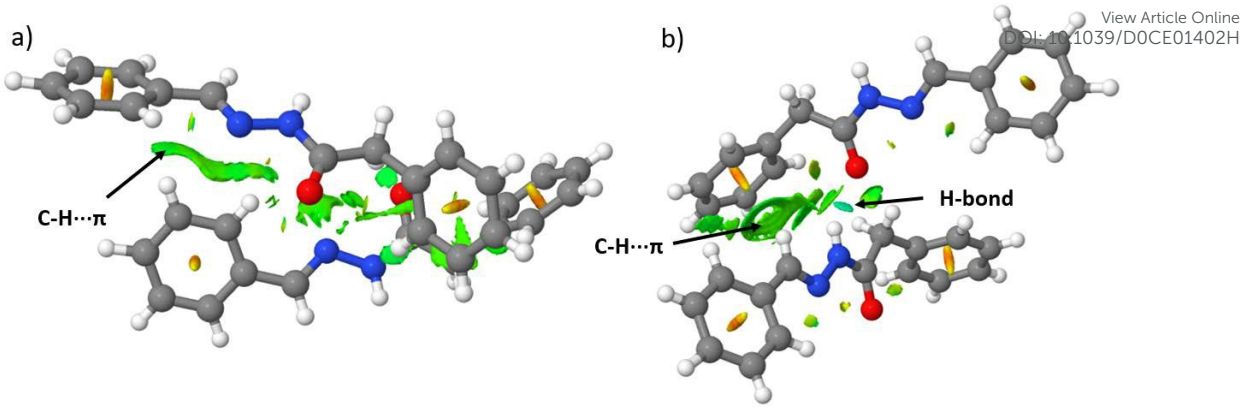

Figure 8. NCI plots of the two dimers of compound **2**. The gradient cut-off is 0.35 a.u. and the color scale is $-0.4 < \rho < +0.4$ a.u.

3.6. *In vitro Lipoxygenase Inhibition Activity of Compounds 1-3.*

Lipoxygenases (EC 1.13.11.12, linoleate: oxygen, oxidoreductases, LOXs) which are widely distributed in plants, animals, and fungi, are a huge monomeric protein family with non-heme, non-sulphur, iron cofactor containing dioxygenases that catalyze the oxidation of polyunsaturated fatty acids (PUFA) as substrate with at least one 1*Z*, 4*Z*-pentadiene moiety such as linoleic, linolenic and arachidonic acid to yield hydroperoxides **[54]**.

Therapeutic efficacy of the synthesized compounds for the inflammation depends upon the inhibition of LOX. The substituted alkoxybenzylidene benzohydrazides (**1** and **3**) and alkoxybenzylidene)-2-phenylacetohydrazide (**2**) were evaluated against soybean lipoxygenase enzyme using indomethacin as a standard drug (IC_{50} = 48.25±1.71 µM) (**Table 5**). Compound **3** bearing 4-nitro functionality displayed better activity in comparison to the standard indomethacin (IC_{50} = 45.31±2.11 µM) (Table 5) while compounds **1** and **2** showed less activity as compared to indomethacin. Structure activity relationship shows that the substituted alkoxybenzylidene benzohydrazides (**1** and **3**) were found to inhibit Lipoxygenase enzyme to a greater extent as compared to alkoxybenzylidene)-2-phenylacetohydrazide (**2**) which also depicts that activity is greater when both the aryl rings are conjugated to central hydrazine moiety (compounds **1** and **3**) as compared with **2** when conjugation is discontinued in case of phenyl acetohydrazide. Putative binding modes and comparison of binding interactions can further be analyzed by molecular docking studies.

Published on 07 December 2020. Downloaded by Goteborgs Universitet on 12/16/2020 11:14:45 AM.

CrystEngComm Accepted Manuscript

View Article Online
DOI: 10.1039/D0CE01402H

Table 5. Inhibitory activity of the alkoxy aryl hydrazones **(1-3)** evaluated against soybean lipoxygenase enzyme.

Compound	Structure	IC_{50} (µM)
1	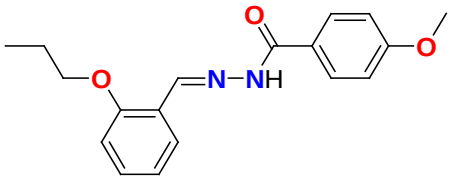	53.52±2.31
2	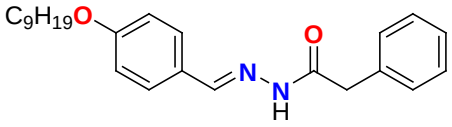	60.33±2.62
3	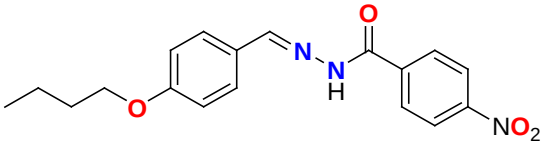	45.31±2.11
	Indomethacin	48.25±1.71

3.7. *Molecular docking Studies*

The *N*-aroylhydrazones (NAH) moiety has been known for their amide and imine functions, NAH compounds may exist as C=N double bond stereoisomers (*E*/*Z*) and as syn/antiperiplanar conformers/rotamers about the amide CO-NH bond. As is evident experimentally from their crystal structures that all the three compounds exist as *E* stereoisomers in their most stable antiperiplanar conformation. Therefore, the molecular docking studies in complex with lipoxygenase enzyme was carried out using antiperiplanar conformations of *E* isomers for binding studies.

The difference between inhibitory activities of analogues studied in this work led us to make structural comparisons in terms of their intermolecular interactions that mediate protein-ligand binding, their relative location in active site, their size, shape, physicochemical properties, *etc*. In order to investigate the binding mode of the inhibitors and their interaction with amino acid residues of lipoxygenase (PDB ID: 1IK3), molecular docking study of synthesized compounds was performed. Docking study further assisted in the identification of the relative location of the co-crystallized inhibitors and reference molecule in the protein architecture of lipoxygenase. Indomethacin was used as the reference drug in biological screening; therefore, it was also docked with the enzyme to know its binding interaction. Results were analyzed and discussed below.

Published on 07 December 2020. Downloaded by Goteborgs Universitet on 12/16/2020 11:14:45 AM.

CrystEngComm Accepted Manuscript

View Article Online
DOI: 10.1039/D0CE01402H

Published on 07 December 2020. Downloaded by Goteborgs Universitet on 12/16/2020 11:14:45 AM.

3.7.1. Druglikeness

Descriptors such as number of rotatable bonds, hydrogen bond donors, hydrogen bond acceptors, Lipinski's acceptors, Lipinski's donors, Lipinski's violation, Lipinski's druglikeness, log*P*, molecular weight and total polar surface area (TPSA) were computed to access the druglike properties of the synthesized compounds. *In silico* calculation results revealed that all the synthesized compounds fulfilled the Lipinski's Ro5 **[55]** and Veber's Ro3 **[56]** cut-off limits, which paved the way towards their capability of inhibiting the activities against lipoxygenase.

The molecules to be considered as drug like must have molecular weight ≤ 500, *log P* (logarithm of the octanol/water partition coefficient) ≤ 5, total polar surface area (TPSA) < 140 Å², number of hydrogen bond donors (HBD) ≤ 5 and hydrogen bond acceptor (HBA) ≤ 10, as per Lipinski's Ro5 **[55]**. Veber *et al* offered further modifications in Ro5 **[56]**. According to Veber, number of rotatable bonds (NOR) of a druglike molecule should be fewer or equal to 10 **[55]**. Molecules which violate more than one of these criteria may have problems with their bioavailability. Detailed results of druglikeness of the hydrazones under study are tabulated in **Table 6**. It has been observed that all the compounds fulfill the criteria to be considered as drug-like molecules as shown in Table 6. The Log P value of the compounds indicates good absorption of hydrazones (**1-3**). After analysis physicochemical properties, the compounds are subjected to docking analysis.

Table 6. Drug-likeness descriptors of the compounds **1-3**.

Physicochemical Property descriptor	**Compound 1**	**Compound 2**	**Compound 3**	**Indomethacin**
Formula	$C_{18}H_{20}N_2O_3$	$C_{24}H_{32}N_2O_2$	$C_{18}H_{19}N_3O_4$	$C_{19}H_{16}ClNO_4$
Molecular weight (g/mol)	312.36	380.52	341.36	357.79
NoR	8	14	9	5
HBA	4	3	5	4
HBD	1	1	1	1
Log P (o/w)	3.41	4.61	3.06	2.76
TPSA	59.92 Å²	50.69 Å²	96.51 Å²	68.53 Å²

Abbreviations used: NoR= Number of rotatable bonds; **HBA**= Hydrogen bond acceptor; **HBD** = Hydrogen bond donor; **Log P** (Log P (o/w)) = logarithm of the (octanol/water) partition coefficient; **TPSA** = Total polar surface area.

CrystEngComm Accepted Manuscript

View Article Online
DOI: 10.1039/D0CE01402H

Published on 07 December 2020. Downloaded by Goteborgs Universitet on 12/16/2020 11:14:45 AM.

3.7.2. Lipoxygenase Structure

The first crystal structure of a LOX **[57]** from Soybean, described by Boyington *et al.*, established the molecular framework common to both plant and animal enzyme. Crystal structure of lipoxygenase bears two major domains: an amino terminal β-barrel, now known as a PLAT (Polycystin-1, Lipoxygenase, Alpha-Toxin) domain and a much larger α-helical domain that houses the catalytic iron **[58]**. The plant enzymes are significantly larger than the animal enzymes (~900 vs. ~650 amino acids, respectively), and the smaller animal enzymes are simply trimmed down by the omission of several plant-specific loop regions. Despite the differences, a large helical core, along with the relative placements of most of the ~17 helices that comprise it, is conserved. At the heart of the core is the catalytic iron, positioned by invariant histidine side chains contributed by the two longest helices in the common core as well as the main chain carboxyl at the C-terminus provided by an invariant Ile. An unusual structural feature of helix α8, a unique insertion which gives it a distinct curvature **[59]** has been observed in all LOX structures to date. Some inhibitors have been reported to bind either directly or indirectly to the adjacent amino acid residues of cofactor **[60-62]**.

3.7.3. Molecular docking and Binding Analysis

For elucidation of the molecular basis of the mechanism of inhibition for synthesized hydrazones (**1-3**), the compounds were docked computationally to the active site of soybean LOX. In this study, first the protein structure (1IK3: 2.0 Å) was retrieved from Protein Data Bank (PDB). The protein was already bound with four ligands in its crystal structure i.e. 13(*S*)-hydroperoxy-9(Z),11(E)-octadecadienoic acid; 13(R)-hydroperoxy-9(Z),11(E)-octadecad ienoic acid; (trans-12,13-epoxy)-9-hydroxy-10(*E*)-octadecenoic acid; trans-12,13-epoxy)-11-hydroxy-9(z)-octadecenoic acid along with Fe(III) as a cofactor. The prominent amino acid residues involved in non-bonding interactions are Phe576, Ser510, Ile572, Arg726, HOH870, Gly720, His513, His518, His523, Leu565, Leu560, Ile557, Ile857, Leu277, Leu773 and Ile772 in the α-helical domain. The bound cocrystallized ligands were removed from active pocket of protein keeping the cofactor iron (Fe^{3+}) intact to study the inhibition mechanism of the active compounds.

To investigate the orientation of synthesized compounds, (*E*)-*N'*-(2-propoxybenzylidene)-4-methoxybenzohydrazide **(1)**, (*E*)-N'-(4-(nonyloxy)benzylidene)-2-phenylacetohydrazide **(2)**, (*E*)-*N'*-(4-butoxybenzylidene)-4-nitrobenzohydrazide **(3)** and the reference compound indomethacin in the active pocket, all compounds were

CrystEngComm Accepted Manuscript

View Article Online
DOI: 10.1039/D0CE01402H

docked into the active site of LOX (PDB code: 1IK3) using Autodock Vina. The results of molecular docking calculations were recorded in 20 different conformations for each compound. Most of the favored conformations occupy pocket area towards α-helical domain however some of the less favored conformations occupied the peripheral region towards the PLAT domain. Variants with the minimal energy of enzyme–inhibitor complex were chosen for further study.

Published on 07 December 2020. Downloaded by Goteborgs Universitet on 12/16/2020 11:14:45 AM.

Table 7. Inhibitory activity against LOX and binding affinity of all ligands.

Compound	Structure	IC_{50} (μM)	Binding affinity (Kcal/mol)
1	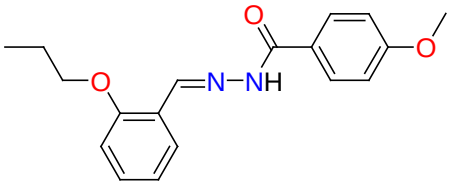	53.52±2.31	-8.7
2	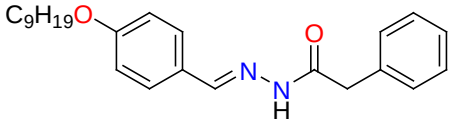	60.33±2.62	-8.2
3	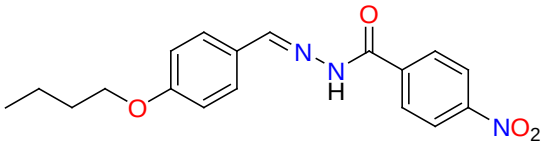	45.31±2.11	-9.6
	Indomethacin	48.25±1.71	-8.3

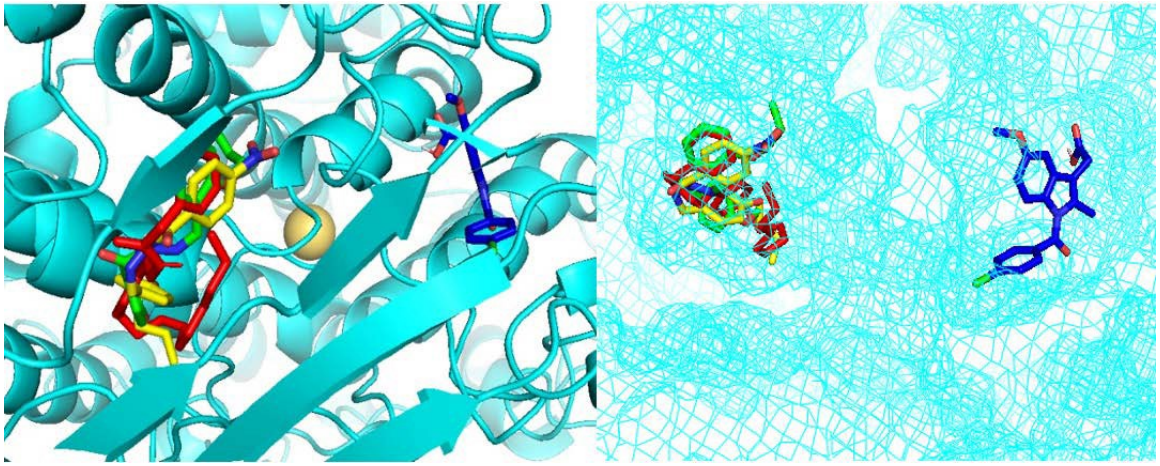

Figure 9. An overlay of the docked orientations of the most preferred conformations of compounds 1, 2, 3 and indomethacin in the active pocket of lipoxygenase (cyan) shown in ribbons (Left). Mesh surface view of ligands enzyme complex (Right). Relative

CrystEngComm Accepted Manuscript

View Article Online
DOI: 10.1039/D0CE01402H

positioning of all 3 variants in the active pocket was shown. Minimal energy conformations of indomethacin were shown in blue and compounds 1, 2 and 3 were shown in green, red and yellow, respectively.

Figure 9 illustrates the relative positioning of hydrazones **1-3** and indomethacin in their minimal energy conformation (out of 20 different conformations for each compound) in the active site of Lipoxygenase. The corresponding binding energies of ligands with most preferred conformation are shown in **Table 7**. As can be seen, the hydrazones **1-3** preferred to bind the enzyme at a place different in position to that for indomethacin owing to the fact that hydrazones are different in structure than indomethacin (Figure 9). Compounds **1-3** have potential to block the entry of substrate by binding to amino acid residues lying near the pocket opening of α-helical domain. A more bent conformation is adapted by **2** (red) (Figure 9) as compared to **1** (green) (Figure 9). The enzyme/inhibitor complexes are stabilized by hydrogen bonds in the hydrophilic region and by π···π and vdW interactions in the hydrophobic region. It has been observed from the binding interactions that the hydrazones interact differently as compared to the interactions of indomethacin (**Figure 9**) owing to the different structures of compounds **1-3** bearing hydrazone moiety as compared to carboxylic acid moiety of indomethacin along with other structural differences besides their positioning in pocket architecture (**Figure 9**).

Published on 07 December 2020. Downloaded by Goteborgs Universitet on 12/16/2020 11:14:45 AM.

CrystEngComm Accepted Manuscript

View Article Online
DOI: 10.1039/D0CE01402H

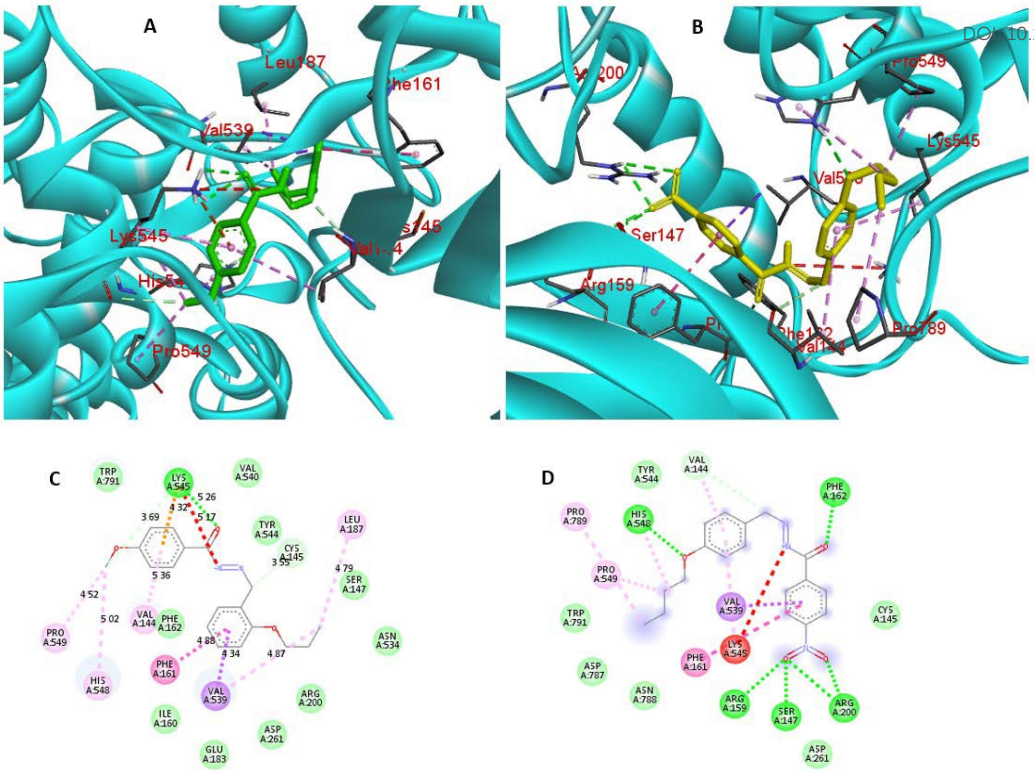

Figure 10. Docking pose of ligands in 3D and 2D display; A) Compound **1** (green), B) Compound **3** (yellow). Ligands are shown in stick mode while receptor is shown in cyan colored ribbons and key residues are shown in stick mode. 2D-Interaction diagram of compound 1 and 3 are represented in C and D, respectively.

The reason for high inhibitory activity of compound **3** as compared to other analogs can be explained by molecular docking studies (**Figure 10**). Compound **3** showed pronounced hydrogen bond interactions as compared to compounds **1**, **2** and indomethacin. The oxygen of butyloxy chain forms hydrogen bond with His548 at a distance 2.52 Å, while the oxygen of hydrazone moiety forms hydrogen bond with main chain amide of Phe162. The greater binding affinity of this hydrazine is mainly attributed to the presence of a nitro group in the phenyl ring of hydrazide moiety. The nitro group plays an important role by forming four hydrogen bonds with the nearby polar residues. Both the oxygens of nitro functionality form hydrogen bonds with Arg200 at a distance of 2.67 Å and 2.85 Å. In addition, the NH of Arg159 forms hydrogen bond with the O-atom of nitro group. The interactions of positive Arginine residue with the negative nitro functionality can also be considered as salt bridge interactions. In addition, the fourth hydrogen bond is formed between oxygen of nitro functionality and Ser147. All these types of hydrogen bonds enhance the binding of this ligand with the lipoxygenase active site in comparison to other

Published on 07 December 2020. Downloaded by Goteborgs Universitet on 12/16/2020 11:14:45 AM.

CrystEngComm Accepted Manuscript

View Article Online
DOI: 10.1039/D0CE01402H

ligands. In addition to hydrogen bonding interactions, the molecule interacted with the binding site via π···π stacking, π-alkyl and alkyl-alkyl interations. 4-nitro phenyl moiety of the benzohydraide analog interacts with Phe161 displaying T shaped π···π interaction with a distance of 4.92 Å. Both phenyl rings of compound **3** interact with Val539 (5.04 Å) and Val144 (5.28 Å) showing π-alkyl interactions. However, in **1**, phenyl ring bearing 4-methoxy functionality forms cation···π interaction with Lys545 at a distance of 4.32Å while the phenyl ring bearing propyloxy chain forms T-shaped π···π interactions. The protein-ligand complex was further stabilized by weaker hydrogen bond between Lys545 and the O-atom of hydrazone. In addition some weaker interactions were observed between propyloxy chain of compound **1** and Leu187 and Val539 forming π-alkyl interactions. The analysis showed that compound **3** showed strong hydrogen bonding interactions with target as compared to compound **1** (see Fig. 10).

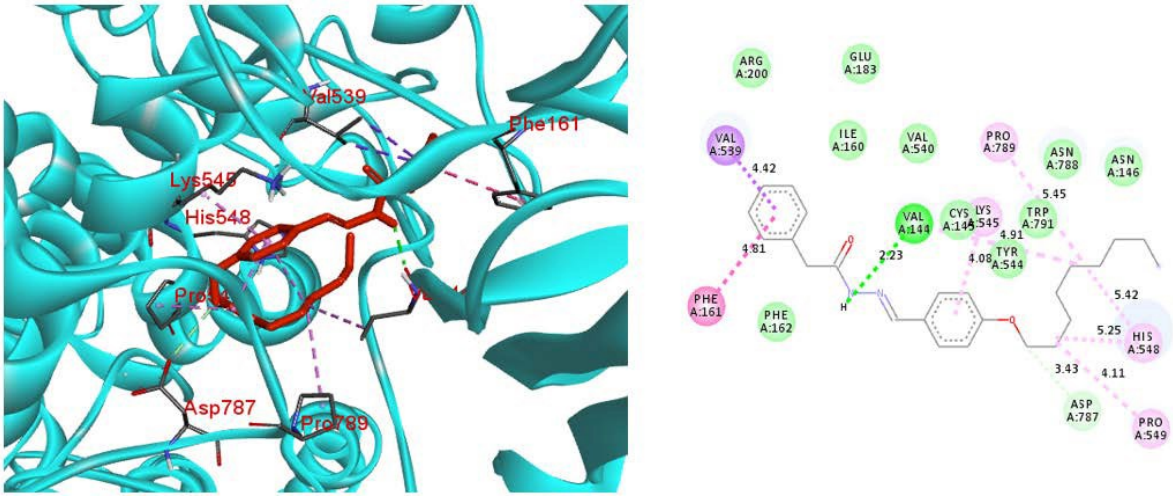

Figure 11. Docking pose of ligand in 3D and 2D display; (Left) Compound **2** (red) shown in stick mode while receptor is shown in cyan colored ribbons and key residues are shown in stick mode. (Right) 2D-Interaction diagram of compound **2**.

Docking analysis of compound **2** is represented in **Figure 11**. As already stated, the hydrazone **2** adopts a bent conformation as there were 14 number of rotatable bonds. In this molecule only one hydrogen bond is observed between the NH and the main chain amide of Val144 at a distance of 2.3 Å. The rest of the interactions observed between **2** and LOX enzyme were pi-alkyl (Pro789, Pro549), pi-sigma (Val539) and vdW interactions (Tyr544, Trp791, Cys145, Val540, Ile160, Glu183). Phenyl ring of hydrazide moiety formed T-shaped π···π stacking with Phe161 residue. Binding analysis showed

Published on 07 December 2020. Downloaded by Goteborgs Universitet on 12/16/2020 11:14:45 AM.

CrystEngComm Accepted Manuscript

View Article Online
DOI: 10.1039/D0CE01402H

that the alkoxy aryl hydrazones **1** and **3** interacted more with polar amino acid residues (Figure 10) however hydrazone **2** showed more interaction with nonpolar amino acid residues (Figure 11). The compound showed weak binding affinity and weaker interactions therefore less active than **1** and **3**.

The docking results showed that compound **3** forms stronger binding interactions with the target molecule followed by compounds **1** and **2**. The molecular docking result is in good agreement with bioactivity data against lipoxygenase. This observation correlates well with the bioassay results, in which compound **3** exhibited higher potency than other ligands because the molecule participates in strong hydrogen bonding interactions with the aforementioned amino acid residues.

4. Conclusions

Three new hydrazide based Schiff bases (**1-3**) have been synthesized and structurally characterized. The crystal structure of compounds **1** and **2** were solved by X-ray diffraction methods. In this work, we have performed a detailed quantitatively analysis on the intermolecular interactions present in the crystal structure of both compounds. The crystal packing of **1** and **2** are stabilized by strong N-H···O hydrogen bonds. In addition, the crystal structure of the compounds shows several relatively weak interactions such as C-H···O, C-H···N hydrogen bonds and C-H···π interactions. In the case of the structure of **2**, weak π···π stacking interactions were observed. This study clearly shows that the energetic distribution in the crystal packing is anisotropic as clearly evident analyzing the energy frameworks diagrams. Analysis of the energy associated with the intermolecular interactions has been also conducted by using DFT calculations and corroborated by NCIplots and QTAIM approach, confirming their importance in the supramolecular assembly of both compounds. In brief, the substituents and the substitution positions play an important role in the packing mode, intermolecular hydrogen bonding and structural conformation of the studied compounds.

All the synthesized substituted alkoxybenzylidene benzohydrazides and phenylacetohydrazides were evaluated against soybean lipoxygenase enzyme using indomethacin as a standard drug. The compounds were found to be the inhibitors of soybean lipoxygenase. Structure activity relationship shows that the substituted alkoxybenzylidene benzohydrazides were found to inhibit Lipoxygenase enzyme to a greater extent as compared to alkoxybenzylidene phenylacetohydrazide. Putative binding modes and comparison of binding interactions of the protein ligand complex were also

Published on 07 December 2020. Downloaded by Goteborgs Universitet on 12/16/2020 11:14:45 AM.

CrystEngComm Accepted Manuscript

View Article Online
DOI: 10.1039/D0CE01402H

analyzed by molecular docking studies in order to rationalize theoretical and experimental studies.

Acknowledgments

MNA is thankful to The University of Azad Jammu and Kashmir for financial support. DMG and MR thank ANPCyT (PICT 2016-0226) and SCAIT-UNT (Project D683) for financial support. M.R. thanks CONICET for the post-doctoral fellowship.

Conflict of Interest

The authors declare no conflicts of interest.

References

1. Z. Albobaledi, M. Hasanzadeh, M. Behzad, A. Abbasi, *Inorg. Chimica Acta*, 2020, 499, 119185.
2. R. Joshi, A. Kumari, K. Singh, H. Mishra, S. Pokharia, *J. Mol. Struct*. 2020, 1206, 127639.
3. M. Rocha, M.C. Ruiz, G.A. Echeverría, O.E. Piro, A.L. Di Virgilio, I.E. León, A. Frontera, D.M. Gil, *New J. Chem*. 2019, 43, 18832-18842.
4. R. Narang, B. Narasimhan, S, Sharma. *Curr. Med. Chem*. 2012, 19, 569-612.
5. O.O. Ajani, C.A. Obafemi, O.C. Nwinyi, D.A. Akinpel, *Biorg. Med. Chem*. 2010, 18, 214-221.
6. S.A. Carvalho, E.F. da Silva, M.V. de Souza, M.C. Lourenço, F.R. Vicente, *Bioorg. Med. Chem. Lett.* 2008, 18, 538-541.
7. S. Zeeshan, M. Naveed, A. Khan, A. Atiq, M. Arif, M.N. Ahmed, Y.S. Kim, S. Khan, *Inflamm. Res.* 2019, 68, 613-632.
8. U. Abu Mohsen, B. Koçyiğit-Kaymakçıoğlu, E.E. Oruç-Emre, Z.A. Kaplancıklı, S. Rollas, Journal of Marmara University Institute of Health Sciences, 2015, 5, 10-14.
9. B. Kaya, Y. Özkay, H.E. Temel, Z.A. Kaplancıklı, *J. Chem*. 2016, 2016.
10. *(a)* P.F. Lamie, W.A.M. Ali, V. Bazgier, L. Rárova. *Eur. J. Med. Chem*. 2016, 123, 803-813; *(b)* M. Ahmed, M. Abdul, Q. Muhammad, I. Shafiq, M. Muddassar, Z. Qadir Samra, A. Hameed, *Arabian J. Chem*. 2019, 12, 41-53; *(c)* V. Kamat, R. Santosh, B. Poojary, S. P. Nayak, B.K. Kumar, M. Sankaranarayanan, Faheem, S. Khanapure, D. Avilla. Barretto, S. K. Vootla. *ACS Omega*, 2020, 5, 39, 25228–

Published on 07 December 2020. Downloaded by Goteborgs Universitet on 12/16/2020 11:14:45 AM.

CrystEngComm Accepted Manuscript

View Article Online
DOI: 10.1039/D0CE01402H

25239; *(d)* M.A. Abdelgawad, M.B. Labib, M. Abdel-Latif, *Bioorg. Chem*. 2017, 74, 212-220.

11. H.J. Schneider, Supramolecular Systems in Biomedical Fields, 1st Ed. RSC Publishing: Cambridge UK, 2013.
12. C.F. Matta, N. Castillo, R.J. Boyd, *J. Phys. Chem. B*, 2006, 110, 563-578.
13. M. Rocha, D.M. Gil, G.A. Echeverría, O.E. Piro, J.L. Jios, S.E. Ulic, *J. Org. Chem*. 2019, 84, 11042-11053.
14. M. Rocha, G.A. Echeverría, O.E. Piro, J.L. Jios, R. Molina, M.E. Arena, S.E. Ulic, D.M. Gil, *Aust. J. Chem*. 2020, 73, 49-60.
15. D. Dutta, S. Mohd, N.U. Islam, U. Saha, A. Frontera, M.K. Bhattacharyya, *J. Mol. Struct.* 2019, 1195, 733-743.
16. D.M. Gil, H. Pérez, G.A. Echeverría, O.E. Piro, A. Frontera, *ChemistrySelect*, 2020, 5, 6331-6338.
17. D.M. Gil, F.F. Salomón, G.A. Echeverría, O.E. Piro, H. Pérez, A. Ben Altabef, *Spectrochim. Acta A*, 2017, 185, 286-297.
18. M.N. Ahmed, B. Sadiq, N.A. Al-Masoudi, K.A. Yasin, S. Hameed, T. Mahmood, K. Ayub, M.N. Tahir, *J. Mol. Struct*. 2018, 1155, 403-413.
19. M.N. Ahmed, K.A. Yasin, S. Hameed, K. Ayub, I.-u. Haq, M.N. Tahir, T. Mahmood, *J. Mol. Struct*. 2017, 1129, 50-59.
20. M.N.Ahmed, M. Arif, F. Jabeen, H.A. Khan, K.A. Yasin, M.N. Tahir, A. Franconetti, A. Frontera, *New J. Chem*. 2019, 43, 8122-8131.
21. G. Sheldrick, SADABS, Program for empirical X-ray absorption correction; Bruker-Nonius: Madison, WI, 1990.
22. G.M. Sheldrick, Crystal structure refinement with SHELXL. *Acta Crystallogr*. 2015, 71C, 3-8.
23. H. Andleeb, I. Khan, A. Bauzá, M.N. Tahir, J. Simpson, S. Hameed, A. Frontera, *Acta Crystallogr*. 2018, 749, 816-829.
24. J.J. McKinnon, D. Jayatilaka, M.A. Spackman, *Chem.Commun*. 2007, 3814-3816.
25. M.A. Spackman, D. Jayatilaka, *CrystEngComm*, 2019, 11, 19-32.
26. M.A. Spackman, *Phys. Scr*. 2013, 87, 048103.
27. J.J. McKinnon, M.A. Spackman, A.S. Mitchel, *Acta Crystallogr*. 2004, 60B, 627-668.

Published on 07 December 2020. Downloaded by Goteborgs Universitet on 12/16/2020 11:14:45 AM.

CrystEngComm Accepted Manuscript

View Article Online
DOI: 10.1039/D0CE01402H

28. M.J. Turner, J.J. McKinnon, S.K. Wolf, D.J. Grimwood, P.R. Spackman, D. Jayatilaka, M.A. Spackman, CrystalExplorer17 (2017). University of Western, Australia.
29. M.J. Turner, S. Grabowsky, D. Jayatilaka, M.A. Spackman, *J. Phys. Chem. Lett*. 2014, 5, 4249-4255.
30. C.F. Mackenzie, P.R. Spackman, D. Jayatilaka, M.A. Spackman, *IUCrJ*, 2017, 4, 575-587.
31. M. J. Frisch, G. W. Trucks, H. B. Schlegel, G. E. Scuseria, M. A. Robb, J. R. Cheeseman, G. Scalmani, V. Barone, B. Mennucci, G. A. Petersson, H. Nakatsuji, M. Caricato, X. Li, H. P. Hratchian, A. F. Izmaylov, J. Bloino, G. Zheng, J. L. Sonnenberg, M. Hada, M. Ehara, K. Toyota, R. Fukuda, J. Hasegawa, M. Ishida, T. Nakajima, Y. Honda, O. Kitao, H. Nakai, T. Vreven, J. A. Montgomery, Jr., J. E. Peralta, F. Ogliaro, M. Bearpark, J. J. Heyd, E. Brothers, K. N. Kudin, V. N. Staroverov, R. Kobayashi, J. Normand, K. Raghavachari, A. Rendell, J. C. Burant, S. S. Iyengar, J. Tomasi, M. Cossi, N. Rega, J. M. Millam, M. Klene, J. E. Knox, J. B. Cross, V. Bakken, C. Adamo, J. Jaramillo, R. Gomperts, R. E. Stratmann, O. Yazyev, A. J. Austin, R. Cammi, C. Pomelli, J. W. Ochterski, R. L. Martin, K. Morokuma, V. G. Zakrzewski, G. A. Voth, P. Salvador, J. J. Dannenberg, S. Dapprich, A. D. Daniels, Ö. Farkas, J. B. Foresman, J. V. Ortiz, J. Cioslowski, and D. J. Fox, Gaussian 09 (Gaussian, Inc., Wallingford CT, 2009).
32. A.D.A. Becke, *J. Chem. Phys*. 1993, 98, 1372-1377.
33. C. Lee, W. Yang, R.G. Parr, *Phys. Rev. B*, 1988, 37, 785-789.
34. P. Elliot, F. Furche, K. Burke, *Rev. Comp. Chem*. 2009, 26, 91-165.
35. S. Grimme, J. Antony, S. Ehrlich, H. Krieg, J. *Chem. Phys*. 2010, 132, 154104.
36. R.F.W. Bader, Atoms in Molecules: A Quantum theory, Oxford University Press, Oxford, UK, 1990.
37. J. Biegler-König, J. Schönbohm, D. Bayles, *J. Comput. Chem*. 2001, 22, 545-559.
38. J. Contreras-García, E.R. Johnson, S. Keinan, R. Chaudret, J.P. Piquemal, D.N. Beratan, W. Yang, *J. Chem. Theory Comput*. 2011, 7, 625-632.
39. *(a)* M. Bharanidharan, S. Manivarman, G. Prabakaran, *Materials Today: Proceedings*, 2020, https://doi.org/10.1016/j.matpr.2020.08.699; *(b)* H. Allgayer, J. Eisenburg, G. Paumgartner. *Eur. J. Clin. Pharmacol*. 1984, 26, 449–451; *(c)* C. Koukoulitsa, D. Hadjipavlou–Litina, G.D. Geromichalos, H. Skaltsa, *J. Enz. Inhib. Med. Chem.* 2007; 22(1), 99–104.

Published on 07 December 2020. Downloaded by Goteborgs Universitet on 12/16/2020 11:14:45 AM.

CrystEngComm Accepted Manuscript

View Article Online
DOI: 10.1039/D0CE01402H

40. U.S. Akula, B. Odhav, *J. Med. Plants Res.* 2008, 2(9), 207-212.
41. S. Sekhar, K. Sampath Kumara, S. Niranjana, H. Prakash, *Int. J. Pharm. Pharm. Sci*. 2013, 5 , 257-262.
42. O. Trott, A.J. Olson, *J. Comput. Chem*. 2010, 31, 455-461.
43. M.F. Sanner, *J. Mol. Graph. Mod*. 1999, 17, 57-61.
44. N.M. O'Boyle, M. Banck, C.A. James, C. Morley, T. Vandermeersch, G.R. Hutchison, J. Cheminform. 2011, 33, 1-14.
45. The PyMOL Molecular Graphics System, Version 1.2r3pre, Schrödinger, LLC.
46. E.F. Pettersen, T.D. Goddard, C.C. Huang, G.S. Couch, D.M. Greenblatt, E.C. Meng, T.E. Ferrin, *J. Comput. Chem*. 2004, 25, 1605-1612.
47. A. Daina, O. Michielin, V. Zoete,. SwissADME: a free web tool to evaluate pharmacokinetics, drug-likeness and medicinal chemistry friendliness of small molecules. Sci Rep. 2017, 7, 42717, 1-13.
48. A. Saeed, M. Ifzan Arshad, M. Bolte, A.C. Fantoni, Z.Y. Delgado Espinoza, M.F. Erben, *Spectrochim. Acta A*, 2016, 157, 138-145.
49. *(a)* S. Parvarinezhad, M. Salehi, S. Kademinia, M. Kubicki, *J. Mol. Struct*. 2019, 1197, 96-107; *(b)* Mamatha S.V., S. Naveen, Zabiulla, Y.H.E. Mohammed, N.K. Lokanath, S.A. Khanum, Chemical Data Collections, 2017, 11-12, 1-10.
50. *(a)* A. Saeed, U. Flörke, A. Fantoni, A. Khurshid, H. Pérez, M.F. Erben, *CrystEngComm*. 2017, 19, 1495-1508; *(b)* A. Saeed, M. Bolte, M.F. Erben, H. Pérez, *CrystEngComm*. 2015, 17, 7551-7563.
51. M.J. Turner, S.P. Thomas, M.W. Shi, D. Jayatilaka, M.A. Spackman, *Chem. Commun.* 2015, 51, 3735-3738.
52. U. Koch, P.L.A. Popelier, J. *Phys. Chem*. 1995, 99, 9747-9754.
53. S. Emamian, T. Lu, H. Kruse, H. Emamian, *J. Comput. Chem*. 2019, 40, 2868-2881.
54. V. Sanda Chedea, M. Jisaka. *InTechOpen*, 2011, 109-130.
55. C.A. Lipinski, F. Lombardo, B.W. Dominy, P. Feeney, *J. Adv. Drug Deliv. Rev.* 1997, 23, 3–25.
56. D.F. Veber, S.R. Johnson, H-Y Cheng, B.R. Smith, K.W. Ward, K.D. Kopple, *J. Med. Chem.* 2002, 45l, 2615–23.
57. D.B. Neau, N.C. Gilbert, S.G. Bartlett, W. Boeglin, A.R. Brash, M.E. Newcomer, *Biochem*. 2009, 48(33), 7906-7915.

Published on 07 December 2020. Downloaded by Goteborgs Universitet on 12/16/2020 11:14:45 AM.

CrystEngComm Accepted Manuscript

View Article Online
DOI: 10.1039/D0CE01402H

58. Y. Xu, A.J. Streets, A.M. Hounslow, U. Tran, F. Jean-Alphonse, A.J. Needham, J.P. Vilardaga, O. Wessely, M.P. Williamson, A.C. Ong, *J. Am. Soc. Nephrol.* 2016, 27(4), 1159-1173.
59. M.E. Newcomer, A.R. Brash, *Protein Sci.* 2015, 24(3), 298-309.
60. E. Skrzypczak-Jankun, J. Chorostowska-Wynimko, S.H. Selman, J. Jankun, *Curr. Enzyme Inhib.* 2007, 3, 119–132.
61. J.C. Boyington, B.J. Gaffney, L.M. Amzel, *Science*, 1993, 260, 1482–1486.
62. C. Charlier, C. Michaux, *Eur. J. Med. Chem*. 2003, 38, 645–659.

Published on 07 December 2020. Downloaded by Goteborgs Universitet on 12/16/2020 11:14:45 AM.

CrystEngComm Accepted Manuscript

View Article Online
DOI: 10.1039/D0CE01402H

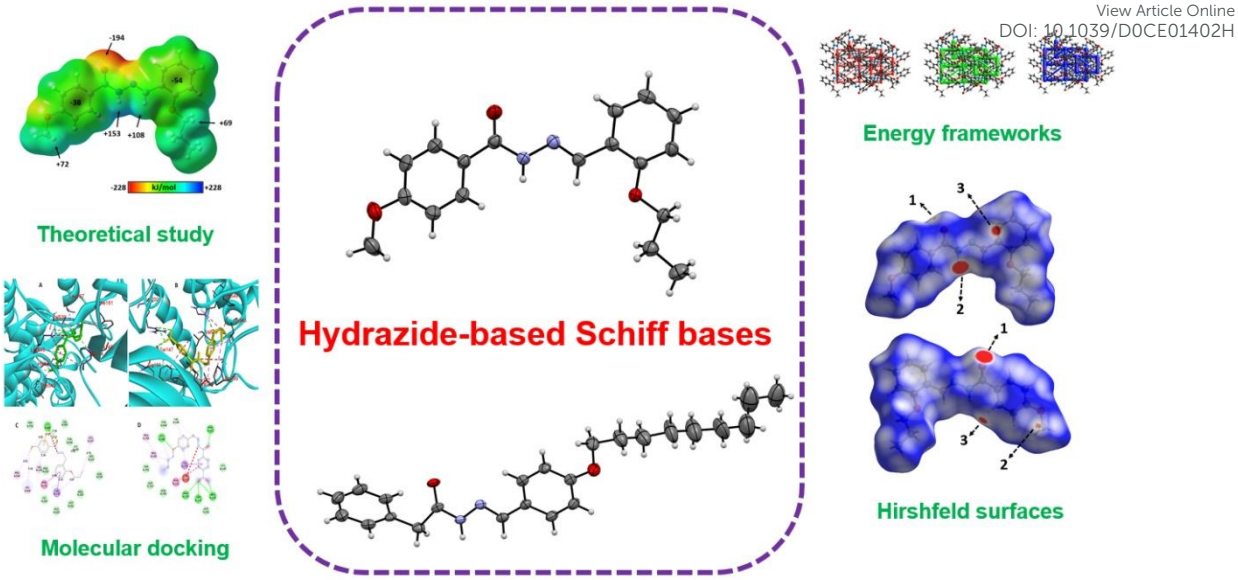

Three Hydrazide-based Schiff bases have been synthesized and characterized by IR, UV-vis and X-ray diffraction methods. A detail analysis of intermolecular interactions has been performed by Hirshfeld surface analysis and DFT calculations.

Published on 07 December 2020. Downloaded by Goteborgs Universitet on 12/16/2020 11:14:45 AM.

CrystEngComm Accepted Manuscript